第43卷 第4期 岩 石 矿 物 学 杂 志 Vol. 43, No. 4: 1012~1033
2024年7月 ACTA PETROLOGICA ET MINERALOGICA July, 2024

·综述与进展·

Doi: 10.20086/j.cnki.yskw.2024.0417

密西西比河谷型(MVT)铅锌矿床与蒸发岩的成因关系

田力丹,宋玉财,庄亮亮,黄 钢
(中国地质科学院 地质研究所, 北京 100037)

摘 要: MVT铅锌矿床的形成与蒸发岩关系密切,但在蒸发盐矿物发生溶解或转变为其他矿物而"消失"时,人们常忽视其曾经存在。本文基于前人研究,对蒸发岩的转变、识别特征及其与MVT铅锌成矿流体来源、硫来源及储矿构造三个方面的关系进行综述。其中,MVT矿床迁移铅锌的盆地卤水主要来自蒸发海水,少量来自蒸发岩的溶解,区域上蒸发岩的发育可指示该区具有成矿流体的发育条件。铅锌金属硫化物中的硫均来自于硫酸盐还原作用,而石膏和硬石膏等蒸发盐矿物是硫酸盐的重要提供者。蒸发岩溶解垮塌利于形成角砾岩与垮塌空间,铅锌矿化可赋存于角砾岩内或其邻近岩层中;盐底辟构造会形成有利于流体聚集和矿质沉淀的构造/化学圈闭,铅锌矿化赋存于底辟体顶部冠岩、边部过渡层和围岩、直立的底辟角砾筒或侧向底辟形成的穹隆体顶部。此外,蒸发盐矿物的假晶、残留的蒸发盐矿物是"消失"蒸发岩存在的直接证据,钠长石和方柱石、正延性玉髓/燧石、富碱土元素双锥状石英等,可指示蒸发岩曾经存在;蒸发岩溶解垮塌构造具有顺地层延伸长等特点,盐底辟构造具有穿层及角砾来自下部层位等特点,是可以协助识别蒸发岩的相关构造。可以看出,区域地层记录有蒸发沉积环境是MVT铅锌成矿必要条件,蒸发岩溶解垮塌和底辟构造是重要找矿目标。

关键词: 蒸发岩; MVT矿床; 卤水; 硫源; 溶解垮塌构造; 盐底辟构造
中图分类号: P618.42; P618.43 **文献标识码**: A **文章编号**: 1000-6524(2024)04-1012-22

Genetic relationship between Mississippi Valley-type (MVT) lead-zinc deposit and evaporite: A review

TIAN Li-dan, SONG Yu-cai, ZHUANG Liang-liang and HUANG Gang
(Institute of Geology, Chinese Academy of Geological Sciences, Beijing 100037, China)

Abstract: Mississippi Valley-type (MVT) lead-zinc deposits are closely related to evaporite rocks, however, the fact that evaporite minerals dissolve or transform into other minerals and "disappear" is often overlooked. Drawing on previous research results, we summarized the transformation and identification characteristics of evaporite, and its relationship with MVT Zn-Pb mineralization that is reflected in the source of mineralizing fluids, the source of sulfur, and the ore-bearing structures. The formation of MVT deposits involves basin brines, primarily derived from evaporated seawater, with a small portion originating from the dissolution of evaporite rocks. Meanwhile, the development of regional evaporite rocks indicates the formation conditions for mineralizing fluids. The sulfur in lead-zinc metal sulfides totally comes from the reduction of sulfates, and evaporite minerals, such as gypsum, anhydrite, etc., are important suppliers of sulfates. Moreover, dissolution-collapse evaporites form breccias and collapse

收稿日期: 2024-03-11; **接受日期**: 2024-05-20; **编辑**: 尹淑苹
基金项目: 国家重点研发计划项目(2021YFC2901805); 国家自然科学基金项目(42125204, 92155305, 42163007)
作者简介: 田力丹(1993-), 女, 博士研究生, 从事矿床学研究, E-mail: tianlidan65@outlook.com; 通讯作者: 宋玉财(1978-), 男, 研究员, 从事矿床学研究, E-mail: song_yucai@aliyun.com。
网络首发时间: 2024-05-27; **网络首发地址**: http://kns.cnki.net/kcms/detail/11.1966.P.20240526.0932.002.html

spaces, and lead-zinc mineralization can occur within the breccias and/or adjacent strata. Salt diapiric structures create favorable structural/chemical traps for fluid accumulation and mineral precipitation, and lead-zinc mineralization can be found in the caprock, transition zones and peridiapiric rocks of salt diapirs, vertically oriented salt diapiric breccia pipes, or top of domes formed by lateral salt diapirism. Pseudomorphs after evaporite minerals and residual evaporite minerals are direct evidence of the existence of "disappeared" evaporites, while minerals such as albite and scapolite, length-slow chalcedony/quartz, alkali-enriched double-terminated quartz, etc., may indicate the past existence of evaporites. The evaporite dissolution-collapse structures exhibit the characteristics of lateral extension along with the stratigraphic strike, and salt diapiric structures have features such as cross-cutting and breccias derived from lower strata, both of which can help identify evaporite-related structures. In exploration for MVT deposits, the regional stratigraphic record of evaporative sedimentary environments is necessary for MVT mineralization, and evaporite dissolution-collapse structures as well as salt diapiric structures are important prospecting targets.

Key words: evaporite; MVT deposit; brine; source of sulfur; dissolution-collapse structure; salt diapir

Fund support: National Key Research and Development Plan (2021YFC2901805); National Natural Science Foundation of China (42125204, 92155305, 42163007)

密西西比河谷型(Mississippi Valley-type, MVT)矿床是全球最重要的铅锌矿床类型之一,属于后生热液矿床,系低温(70~250℃)、中-高盐度(10%~30%)的盆地卤水在沉积盆地中迁移并萃取金属,最终以铅锌硫化物形式沉淀于碳酸盐岩(少量为碎屑岩)中成矿,与岩浆活动无直接成因关系(Leach *et al.*, 2005)。

MVT 铅锌成矿与蒸发岩关系密切。早期研究强调,蒸发岩与铅锌成矿流体及硫的来源有关。由于迁移铅锌的盆地卤水主要来自海水蒸发,也可能有来自地层中蒸发岩溶解的贡献(Kesler *et al.*, 1996; Viets *et al.*, 1996; Chi and Savard, 1997),预示着 MVT 矿床所在盆地曾发生有蒸发作用并可能形成了蒸发岩;有机质等还原(溶解的)石膏和硬石膏等蒸发岩可为铅锌成矿提供还原硫(Sangster, 1990; Leach *et al.*, 2005)。早期研究也注意到,一些 MVT 矿床的就位与蒸发岩溶解垮塌及蒸发岩底辟构造有关(Tompkins *et al.*, 1994a, 1994b; Kyle and Saunders, 1996; Kyle and Misi, 1991; Warren and Kempton, 1997; Velasco *et al.*, 2003; Kesler and Reich, 2006; Bouhlel *et al.*, 2016)(图 1),但并未引起足够重视。近年来,有学者对我国金顶和境内其他一些 MVT 铅锌矿床研究后,强调这两类构造是 MVT 矿床非常重要的储集空间(Leach *et al.*, 2017; Leach and Song, 2019),随后全球其他地区的一些研究也进一步强化了这一认识(de Oliveira *et al.*, 2019; Rddad *et al.*, 2019; Song *et al.*, 2020; Tian *et al.*, 2022; Rosa *et al.*, 2023; Zhuang *et al.*, 2023)。尽管如此,由于蒸发盐矿物易溶解和易被其他矿物交代(Warren, 2000, 2016),以致其地质记录往往"消失",故蒸发岩常常未被识别而导致人们忽略它在成矿中的重要性。

本文首先介绍蒸发岩基本特征、属性及如何识别"消失"的蒸发岩,然后介绍蒸发岩在提供成矿卤水和还原硫方面的作用,重点阐述与蒸发岩有关的储矿构造并介绍矿床实例,最后进行了总结。系统梳理了蒸发岩与 MVT 铅锌成矿的关系,强调要重视蒸发岩,特别是其作为储矿构造在 MVT 铅锌成矿和找矿中的重要性。

1　蒸发岩的基本概念

狭义上,蒸发岩(evaporite)指由蒸发作用下地表或近地表卤水饱和而沉淀出的一类含盐岩石,Warren(1996)将其归类为原始蒸发岩(primary evaporites)。广义上,蒸发岩还包括形成于同沉积作用或埋藏成岩过程中对原始蒸发盐矿物交代、溶蚀或再沉淀等作用形成的蒸发岩,即次生蒸发岩(secondary evaporites)以及热液蒸发岩。

广义上,蒸发盐矿物包括蒸发碳酸盐岩(evaporitic carbonates),主要有文石($CaCO_3$)、方解石($CaCO_3$)、白云石[$Ca_{(1+x)}Mg_{(1+x)}(CO_3)_2$]、菱镁矿($MgCO_3$)等,以及硼酸盐、硝酸盐、复盐类矿物等。狭义上,蒸发盐矿物仅指石膏($CaSO_4 \cdot 2H_2O$)、硬石

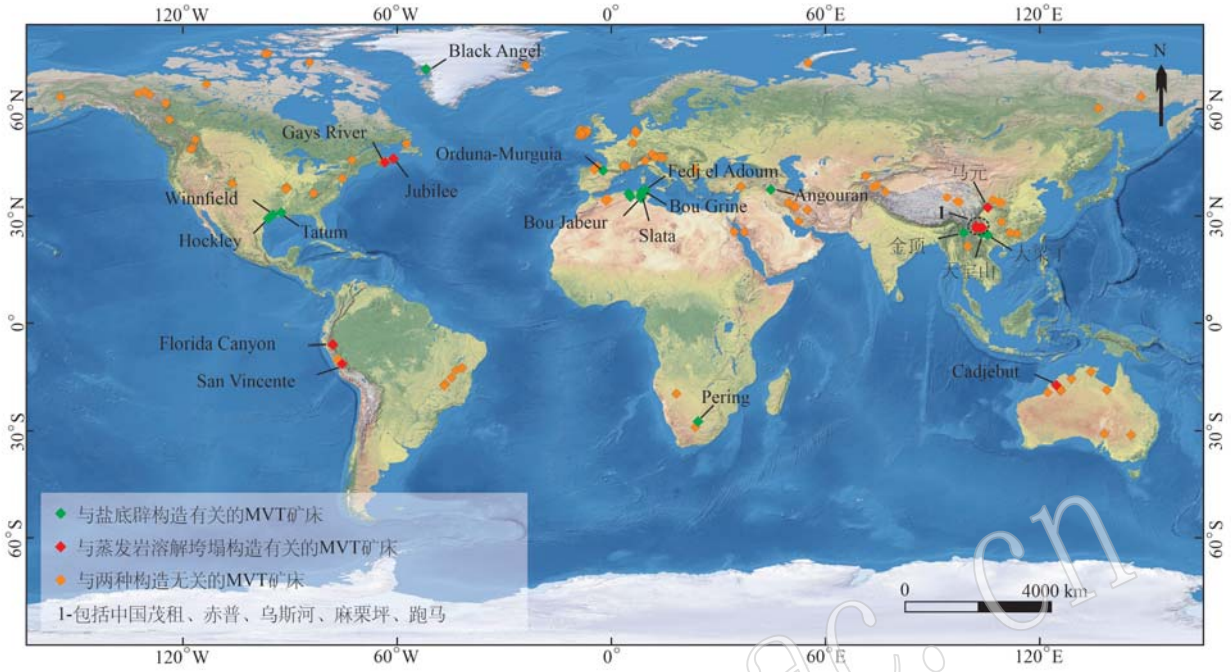

图 1 全球 MVT 铅锌矿床分布(地图来源 http://www.naturalearthdata.com/)

Fig. 1 Global distribution of MVT Zn-Pb deposits (source of map: http://www.naturalearthdata.com/)

MVT 铅锌矿床数据来源于 Taylor *et al.*, 2009;与蒸发岩溶解垮塌构造有关的矿床据 Tompkins *et al.*, 1994a; Warren and Kempton, 1997; Warren, 2000; Leach and Song, 2019; Tian *et al.*, 2022;与蒸发岩底辟构造有关的矿床据 Rouvier *et al.*, 1985; Kyle and Posey, 1991; Kyle and Saunders, 1996; Bouhlel *et al.*, 2007, 2009, 2016; Bouabdellah *et al.*, 2014, 2015; Perona *et al.*, 2018; Leach and Song, 2019; Rddad *et al.*, 2019; Rosa *et al.*, 2023; Zhuang *et al.*, 2023

data of MVT deposits from Taylor *et al.*, 2009; evaporite dissolution-collapse structure-related MVT deposits from Tompkins *et al.*, 1994a; Warren and Kempton, 1997; Warren, 2000; Leach and Song, 2019; Tian *et al.*, 2022; salt diapiric structure-related MVT deposits from Rouvier *et al.*, 1985; Kyle and Posey, 1991; Kyle and Saunders, 1996; Bouhlel *et al.*, 2007, 2009, 2016; Bouabdellah *et al.*, 2014, 2015; Perona *et al.*, 2018; Leach and Song, 2019; Rddad *et al.*, 2019; Rosa *et al.*, 2023; Zhuang *et al.*, 2023

膏($CaSO_4$)、石盐(NaCl)、钾盐(KCl)等硫酸盐及氯化物(Kendall, 1978; Miall, 1985; Warren, 1996, 2016),本文涉及的蒸发盐矿物指狭义概念。此外,在中文文献中也常称蒸发岩为膏盐岩(金之钧等, 2006, 2010; 刘家军等, 2007)。

2 蒸发岩的转变及识别

蒸发盐矿物中,氯化钠和氯化钾等在水溶液中溶解度高,而石膏、硬石膏溶解度相对低,但在周围氯化物盐类大量溶解时其溶解速度明显增加(Waltham *et al.*, 2005; Ford and Williams, 2007)。在埋藏成岩或热液活动过程中,蒸发盐矿物易溶解消失或被其他矿物替代(Warren, 2016),故蒸发岩往往难以得到完整的保存,有效地识别"消失"的蒸发岩尤为重要。

在高温或变质条件下,蒸发岩及围岩地层可蚀变形成含钠长石、钾长石、方柱石以及电气石等矿物,尤其在铁氧化物铜金(IOCG)型矿床中常见(Wang *et al.*, 1998; Hitzman, 2000; Williams *et al.*, 2005)。在变质作用过程中,除低级变质绿片岩相中可保留少量硬石膏外,中-高级变质作用下蒸发岩矿物均发生蚀变、重结晶或转变为新的矿物(Spear, 1993)。蒸发岩在变质过程中,是通过外来流体溶解蒸发岩中的 Na、K、Ca、Mg、Cl、B 等组分,迁移并与邻近围岩发生相互作用,形成富钠长石岩、富钾长石岩、富电气石岩、富方柱石岩等(许虹等, 2001; Warren, 2016),这些岩石在高级变质作用后仍可完整保留。但需要注意的是,上述矿物可以在其他条件下形成,仅靠矿物组成并不能直接判断这些岩石与蒸发岩有关,需结合其他证据进行综合分析,如矿物相分布和蚀变分带的产状受蒸发岩地层层序或盐构造控制(Hietanen, 1967; Sharma, 1981)、存在盐类矿物假晶、高盐度流体包裹体组合等(Moine *et al.*,

1981；Roedder，1984；Grotzinger，1986）。

在中、低温条件下，蒸发岩常转变为溶解度更低的碳酸盐岩、硅质或硫酸盐矿物，在 MVT 铅锌矿床中较为常见（Warren，2000，2016）。石膏、硬石膏等硫酸盐矿物的碳酸盐化作用十分普遍，产物以白云石和方解石为主（Kyle and Posey，1991；Anadón *et al.*，1992；Tompkins *et al.*，1994a，1994b；Machel，2001；Gandin *et al.*，2005；Fernández-Díaz *et al.*，2009，2010），其转化机制主要有两种：一种是石膏/硬石膏溶解后被碳酸盐矿物充填（Pierre and Rouchy，1988；Sanz-Rubio *et al.*，2001；Fernández-Díaz *et al.*，2009），此过程可较好地保留原始硫酸盐矿物形态，形成假晶（Fernández-Díaz *et al.*，2009），常见石膏/硬石膏的针柱状、板柱状晶体或放射状、玫瑰花状集合体形态（Tucker，1976；Sanz-Rubio *et al.*，2001；Fernández-Díaz *et al.*，2009）（图 2a）。而当溶解与沉淀作用近同时发生时，碳酸盐矿物则以结核状或透镜状矿物假晶为主（Sanz-Rubio *et al.*，2001；Melezhik *et al.*，2005；Caruso *et al.*，2017）；另一种是在有机质参与下硫酸盐通过生物化学还原（bacterial sulfate reduction，BSR）或热化学还原作用（thermochemical sulfate reduction，TSR）转化为方解石、白云石等矿物（Anadón *et al.*，1992；Machel，2001；Gandin *et al.*，2005），除可能保留有硫酸盐矿物假晶外，形成的碳酸盐矿物的碳同位素值会受到具有较低 $\delta^{13}C$ 值的有机质碳同位素组成（通常 $\delta^{13}C$ 值为−25‰ ~ −30‰ PDB，Machel *et al.*，1995）的影响，而明显降低。值得注意的是，在任何机制下碳酸盐矿物中含硫酸盐矿物包体，是碳酸盐化交代硫酸盐蒸发岩的有力证据（Pierre and Rouchy，1988；Anadónet *et al.*，1992；Fernández-Díaz *et al.*，2009）。此外，球状方解石和板柱状白云石晶体也常形成于富蒸发岩环境（Perkins *et al.*，1994；Sanz-Montero *et al.*，2006；Fernández-Díaz *et al.*，2010；Bots

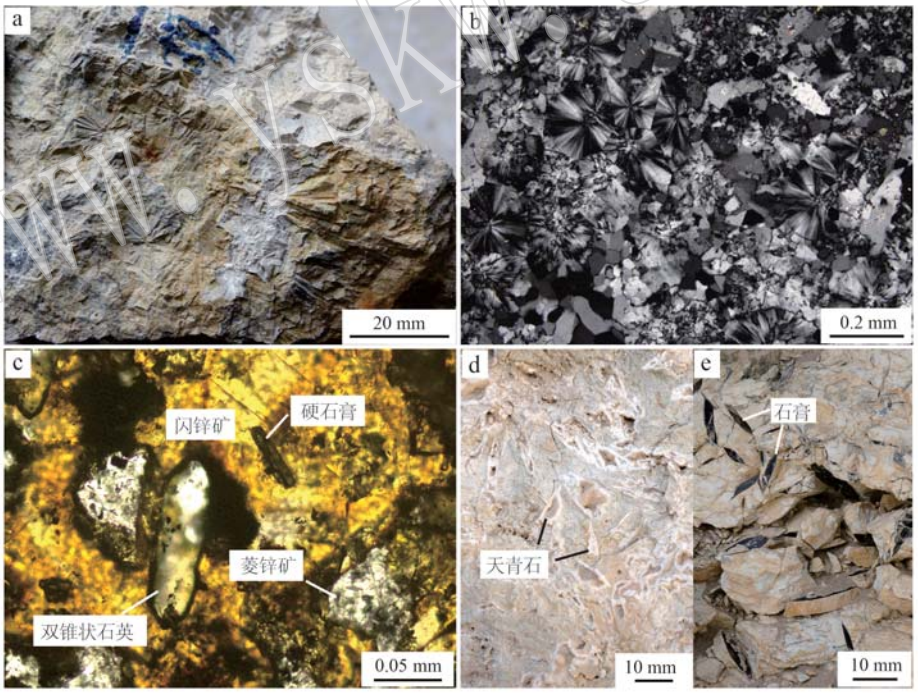

图 2　“消失”的蒸发盐矿物的识别标志

Fig. 2　Identification of “vanish” evaporite minerals

a—方解石呈玫瑰花状石膏假晶，金顶矿床（手标本）；b—放射状正延性玉髓，麻栗坪矿床（正交偏光）；c—自形双锥状石英与硬石膏包裹于闪锌矿中，伊朗 Angouran 矿床（单偏光，Zhuang *et al.*，2023）；d、e—地层中同时发育天青石和石膏，天青石与石膏晶形相似、呈石膏假晶形态，青海大风山锶矿床（露头）

a—rosette-like calcite pseudomorphs after gypsum，Jinding deposit（hand specimen）；b—radial length-slow chalcedony，Maliping deposit（cross-polarized light）；c—double-terminated quartz and anhydrite occur in sphalerite，Angouran deposit（plane-polarized light，Zhuang *et al.*，2023）；d，e—celestite and gypsum occur in the same sedimentary beds，where celestite displays lenticular pseudomorphs after gypsum in the Dafengshan Sr deposit，Qinghai（outcrop）

et al., 2011)。

蒸发岩的硅化作用较为常见,尤其在前寒武白云岩建造中更为普遍(Friedman and Shukla, 1980),以蒸发盐矿物溶解、玉髓或石英等硅质物质交代-充填形式出现(Maliva *et al.*, 2005)。与蒸发岩关系密切的玉髓/燧石往往具正延性,其 *c* 轴与矿物延伸方向一致(Folk and Pittman, 1971; Keene, 1983; Daley, 1989)(图 2b),而常见的石英常为负延性(Siedlecka, 1972)。由于溶解和结晶速度的差异,硫酸盐矿物在硅化作用后,常可保留硫酸盐矿物晶型或集合体形态(Folk and Pittman, 1971; Daley, 1989)。此外,由于蒸发岩具有硬度低、易塑性流动和溶解的特性,当石英在其中生长时,有利于其晶面的完整发育而形成自形的双锥状石英(double-terminated quartz, 图 2c; Friedman and Shukla, 1980; Kyle and Posey, 1991; Ulmer-Scholle *et al.*, 1993; Henchiri *et al.*, 2015; Leitner *et al.*, 2017),石英内部有时可见残余的蒸发盐矿物包体、板状白云石、球形方解石包体等(Ulmer-Scholle *et al.*, 1993; Hechiri *et al.*, 2015; Chen *et al.*, 2016; Zhuang *et al.*, 2023)。自形双锥状石英一般具有高 Al、低 Ti 以及 Li、Na、K 异常富集、B 含量相对较高的微量元素组成特征(Zhuang *et al.*, 2023),前者指示其形成于低温环境(<350℃, Rusk *et al.*, 2008; Lehmann *et al.*, 2011),后者则可能与蒸发岩环境导致的相关元素进入矿物晶格有关(Lehmann *et al.*, 2011; Götze, 2012)。同时,蒸发环境中硫酸盐矿物或强蒸发环境卤水常具有富^{18}O的特点(Henchiri and Slim-S'himi, 2006; Bustillo *et al.*, 2017; Teboul *et al.*, 2019),故该环境下形成的双锥状石英的氧同位素值往往出现高的$\delta^{18}O$值,如在伊朗 Angouran 铅锌矿床,推断为盐底辟角砾岩筒中双锥状石英的$\delta^{18}O$值最高可达 28.3‰(Zhuang *et al.*, 2023)。

蒸发岩的硫酸盐化主要是石膏、硬石膏转变为溶解度较低、更易保存的天青石($SrSO_4$)或重晶石($BaSO_4$)(Carlson, 1987; Scholle *et al.*, 1990; Sullivan and Koppi, 1993; Hanor, 2000, 2004)。其转变方式为硫酸钙矿物发生溶解产生富SO_4^{2-}流体,随后与富Sr^{2+}或Ba^{2+}流体发生混合导致矿物结晶沉淀,或富Sr^{2+}或Ba^{2+}流体直接交代石膏、硬石膏,这时可能保留石膏或硬石膏假晶(图 2d、2e),并包含石膏或硬石膏矿物包体(Sullivan and Koppi, 1993; Hanor, 2000, 2004; Dill *et al.*, 2009)。

3 MVT 矿床成矿流体和硫的来源及与蒸发岩的关系

3.1 成矿流体来源

流体包裹体分析显示,MVT 铅锌矿床成矿流体为低温、中-高盐度的盆地卤水(Leach and Sangster, 1993; Leach *et al.*, 2005; Wilkinson, 2014),这是由于铅锌金属离子主要以氯络合物形式迁移,而高盐度意味着高的 Cl 浓度和强的迁移铅锌能力(Moldovanyi and Walter, 1992; Emsbo *et al.*, 2000; Yardley, 2005)。

对于盆地卤水的起源,Hanor(1979)提出是由地层中蒸发岩的溶解、原生卤水的参与或蒸发地表海水的入渗等过程导致;Rittenhouse(1967)、Carpenter(1978)、Kharaka 等(1987)、Moldovanyi 和 Walter(1992)等通过对现代盆地卤水中溶质含量比值进行计算后,得出卤水中的盐类主要来源于近地表蒸发海水或地下蒸发盐矿物的溶解。Viets 等(1996)和 Kesler(1996)分别对波兰 Silesian-Cracow MVT 铅锌矿集区中成矿期硫化物的流体包裹体组分及美国东部 Appalachian 盆地 MVT 铅锌矿床的闪锌矿流体包裹体 Na-Cl-Br 组成进行了分析,认为成矿流体主要来自于近地表蒸发浓缩后的海水; Chi 和 Savard(1997)利用 Na-Ca 盈亏图解对 Viburnum Trend 和 Gays River 铅锌矿床的成矿流体进行了分析,认为流体来源于蒸发海水并溶解地层中盐类矿物。值得注意的是,上述矿集区及矿床的成矿流体均显示出与各自区域内相关盆地卤水组成相似的特点。统计全球典型 MVT 矿床中闪锌矿流体包裹体的 Cl/Br-Na/Cl 摩尔比值,显示大部分数据点紧邻海水蒸发线(图 3, Leach *et al.*, 2005),流体主要来源于蒸发的海水,部分来自岩盐、石膏等蒸发盐矿物的溶解。上述资料表明,要形成 MVT 成矿流体,矿床所在地区一定经历过强烈的蒸发作用。地层中的蒸发岩即是蒸发作用的地质记录,蒸发岩的发育反映了相应区域具有形成 MVT 铅锌成矿流体的能力,有时通过溶解作用而产生高盐度的卤水。

3.2 还原硫来源

MVT 铅锌矿床的有用矿物是方铅矿和闪锌矿,因此成矿需要还原硫。沉积盆地中的还原硫主要来自硫酸盐的 BSR 或 TSR 作用(Powell and Macqueen

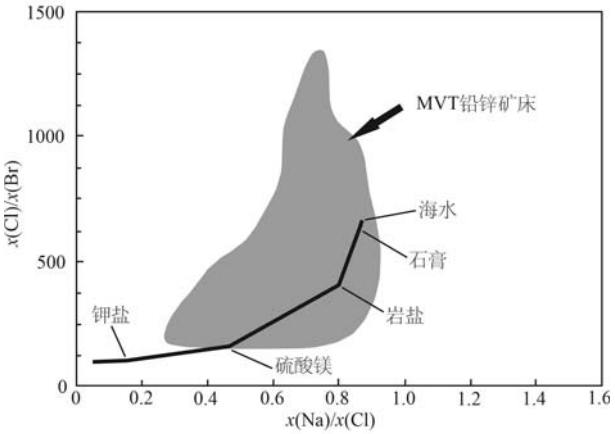

图 3　MVT 矿床闪锌矿中流体包裹体的 Cl/Br-Na/Cl 图解（据 Leach *et al.*, 2005 修改）

Fig. 3　Cl/Br vs. Na/Cl molar ratios of fluid inclusions in sphalerite from the MVT deposits (modified from Leach *et al.*, 2005)

1984; Seal, 2006; Anderson and Thom, 2008)，而地层中的石膏和硬石膏等蒸发岩是硫酸盐的重要来源(Sangster, 1990; Leach *et al.*, 2005)。

BSR 和 TSR 作用都是以有机质作为还原剂，分别是小于 70℃～80℃的厌氧环境下、细菌参与的异化还原作用(Jørgensen *et al.*, 1992; Canfield, 2001)，和大于约 120℃条件下发生的非生物热化学还原作用(Trudinger *et al.*, 1985; Krouse *et al.*, 1988; Ohmoto and Goldhaber, 1997)。硫酸盐在 BSR 或 TSR 过程中不同程度地消耗^{34}S，使得还原硫的 δ^{34}S 值明显降低(Chambers and Trudinger, 1979)，降低程度受控于硫酸盐还原速率、体系为开放或封闭等因素；当体系封闭时，甚至会导致部分硫化物 δ^{34}S 值接近或高于硫酸盐的最高值(Goldhaber and Kaplan, 1975; Seal and Wandless, 2003)。其中，BSR 过程可使硫酸盐和硫化物间的 δ^{34}S 值相差 2‰～42‰，故相关硫化物的 δ^{34}S 值常出现负值且值域较宽(Goldhaber and Kaplan, 1975; Detmers *et al.*, 2001)，而 TSR 过程往往导致两者的 δ^{34}S 值相差小于 15‰，相关硫化物 δ^{34}S 值正、值域较窄(Machel *et al.*, 1995; Ohmoto and Goldhaber, 1997; Seal, 2006)。

统计表明，全球不同时期海水硫酸盐的 δ^{34}S 值总体分布于+10‰～+35‰之间(Claypool *et al.*, 1980; Canfield, 2001, 2004; Seal, 2006; Sharp, 2017)，其可代表地层中石膏和硬石膏的 δ^{34}S 值，而全球 MVT 矿床中闪锌矿的硫同位素值介于-40‰～+35‰之间(Leach *et al.*, 2005; Leach and Song, 2019)，反映了 TSR 和 BSR 均参与了 MVT 矿床还原硫的产生。但对于单个矿床而言，通常以 TSR 或 BSR 一种方式的还原硫来源为主(Leach *et al.*, 2005)。由于迁移铅锌的成矿流体必须贫还原硫(Emsbo *et al.*, 2000)，那么铅锌硫化物沉淀时，还原硫可以① 来自其他流体，TSR 或 BSR 均可以提供，这时通过流体混合成矿；② 来自成矿流体或其他流体中溶解的硫酸盐在成矿时被还原，即“原位还原机制”成矿，这时由于温度高，还原硫由 TSR 作用产生。在矿床内或邻区可能发现石膏或硬石膏被碳酸盐矿物交代，或发现成矿有关碳酸盐矿物的 δ^{13}C 值明显偏低，可指示有机碳参与了碳酸盐矿物的形成(黄世强, 2019)，表明着硫酸盐发生了 BSR 或 TSR 作用。

4　蒸发岩有关的储矿构造

与蒸发岩相关储矿构造，主要源于蒸发岩的溶解垮塌和底辟作用，使富蒸发岩部位和围岩形成较好的孔隙空间，为成矿流体运移、铅锌沉淀及储存提供有利条件。

4.1　蒸发岩溶解垮塌构造

4.1.1　基本特征及识别标志

沉积地层中，蒸发盐矿物的溶解度大于碳酸盐等其他常见矿物，受大气降水或埋藏期不同流体的作用会发生溶解，当溶解速率较慢时仅形成顺层分布次生孔洞，而当快速且大量溶解时则会引起层间或上覆岩石发生垮塌形成蒸发岩溶解垮塌角砾岩(Smith, 1972; Beales and Hardy, 1977; Swennen, 1990; Friedman, 1997)。Warren(2016)总结了此类角砾岩构造的理想模型(图 4)，即：从下至上分别为不溶残留物层(insoluble residues)，角砾岩层(main breccias body)和碎裂层(crackle/mosaic breccias)三个部分。其中，最底部的不溶残留物层位于角砾岩体下盘边缘，由蒸发岩溶解后或层间碳酸盐岩、碎屑岩中的不溶残留物质组成，包括硬石膏或燧石、碎屑石英、菱形白云石及粉砂质、黏土类等矿物，随后被方解石、白云石及硅质等自生矿物胶结，层厚通常较小。如，厚 100 m 蒸发岩层完全溶解后仅产生 50～80 cm 厚残留不溶物层(Smith, 1972)，并与下伏岩层呈突变接触且界线平滑(图 4)。与邻近非蒸发岩沉积物相比，该残留层受机械及化学压实作用影响较小，因此具有更好的渗透率和孔隙度，可作为后期

成矿流体及碳氢化合物的潜在储层。

中部为角砾岩层,厚度约1 ~ 100 m,主体由下至上分别以杂基支撑悬浮角砾岩(float breccia)或碎屑支撑充填角砾岩(rubble/pack breccia)为主(图4),分别形成于同固结程度较差岩石互层、杂质含量较高的蒸发岩溶解,或与坚硬岩石互层的较纯蒸发岩溶解环境中,二者无明显分界线,角砾碎屑来自上覆或层间岩层,呈棱角状,碎屑间并不匹配且延长方向无明显定向性(图4)。另外,岩层底部的部分角砾岩由于溶解垮塌迁移距离较小,几乎为近原地下沉,其破坏程度和延长方向改变较小,因此与原始岩层产状基本一致,局部形成盐内沉积角砾岩薄层(图4)。

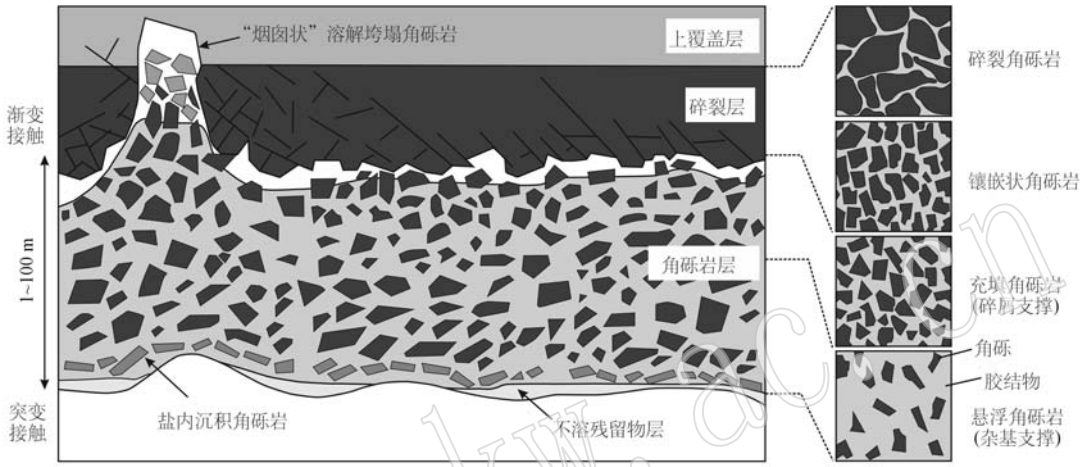

图4 蒸发岩溶解垮塌角砾岩特征理想模型(据Morrow, 1982; Warren, 2016修改)

Fig. 4 Ideal model of evaporite dissolution-collapse breccias (modified from Morrow, 1982; Warren, 2016)

角砾岩层上部呈渐变过渡至碎裂层,这是随着蒸发岩溶解后期岩石破碎作用减弱所致,以碎裂(crackle breccia)或镶嵌状角砾岩(mosaic breccia)为主,二者角砾碎屑位移相对较小、延长方向有定向性且错位不明显(图4)。当角砾碎屑间缺少胶结物充填时,即可成为铅锌成矿及油气资源的优质储集空间。碎裂层顶部仅保留轻微断裂及膨胀作用,直至上覆岩层无明显改造。此外,当蒸发岩大量溶解导致上部发生跨地层垮塌作用时,在角砾岩层顶部及碎裂层中的角砾岩体可显示为"烟囱状"溶解垮塌特征(图4)。

当蒸发岩溶解"消失"时,蒸发岩溶解垮塌角砾岩常与沉积角砾岩、碳酸盐溶解垮塌角砾岩等相混淆,较难识别。一些主要标志可协助识别蒸发岩溶解垮塌角砾岩,包括:① 沉积环境,常分布于浅海碳酸盐台地相(如萨布哈、潟湖相、潮上-潮间带)和高能沉积陆架边缘的碳酸盐岩中(Morrow, 1982; Swennen *et al.*, 1990; Tian *et al.*, 2022)。注意识别蒸发盐矿物假晶,围岩中指示蒸发环境的沉积构造,如斑马构造(zebra texture)、鸟眼构造(bird's eye texture)、穿刺构造、盘肠构造(enterolithic structure)、帐篷构造(antiformal tepee structure)、流动构造等(Beales *et al.*, 1980; Kendall and Warren, 1987; Tompkins *et al.*, 1994b; Sheppard *et al.*, 1996; Jackson *et al.*, 2003; Hearon *et al.*, 2014; Thomas *et al.*, 2015);② 角砾岩体特征,常顺层分布,层位相对稳定,垂向延伸有限,而侧向延伸可达上百米至数十公里,可能断续分布,常与上覆岩层呈渐变接触,而与下伏地层呈突变接触(图4);③ 角砾岩形态及组成,角砾碎屑呈棱角状,碳酸盐岩溶蚀形成的次磨圆状角砾不多见,无分选性,可见较多的长轴较长的角砾,长轴近平行于或斜交地层出现,角砾来自近原位的上覆地层,可"复位"至原始层位,内沉积物较少(Swennen *et al.*, 1990; Warren, 2016; Leach and Song, 2019)。

4.1.2 矿床实例

Cadjebut矿床(矿石3.5 Mt, Pb+Zn品位17%)位于澳洲西北部,赋矿围岩为泥盆系下部Pillara台地碳酸盐岩(Tompkins *et al.*, 1994a; Wallace *et al.*, 1994)(图5a),以鲕粒滩相和潟湖相沉积为主,矿床围岩则处于潟湖相沉积旋回顶部的盐滩或萨布哈亚相中(Warren, 2016)。矿体呈似层状、透镜状顺层

产出，以韵律条带型和角砾岩型矿石为主。尽管矿床内少见蒸发岩，但矿体内部及边缘均可见大量方解石、石英交代的蒸发盐矿物假晶，保留的沉积结构与矿床外围富蒸发岩层位的沉积结构特征对应（图 5b）。角砾岩型矿石包括杂基支撑和角砾碎屑两种，角砾均呈棱角状（图 5c）。条带型矿石发育于具斑马构造的白云岩内，由早阶段细-中晶粒状闪锌矿和晚阶段胶状闪锌矿、树枝状方铅矿组成（Warren and Kempton，1997）。研究认为，成矿流体进入含蒸发岩建造，成矿早期蒸发岩溶解速率小于成矿流体供给沉淀效率，硫化物直接交代白云岩形成韵律条带状矿石；随着溶解速率逐渐增加，超过并远大于硫化物沉淀速率时，蒸发岩发生溶解垮塌作用形成大量孔洞，硫化物充填于角砾间孔隙中，先后形角砾岩型矿石（Tompkins *et al.*，1994a，1994b；Warren and Kempton，1997）。

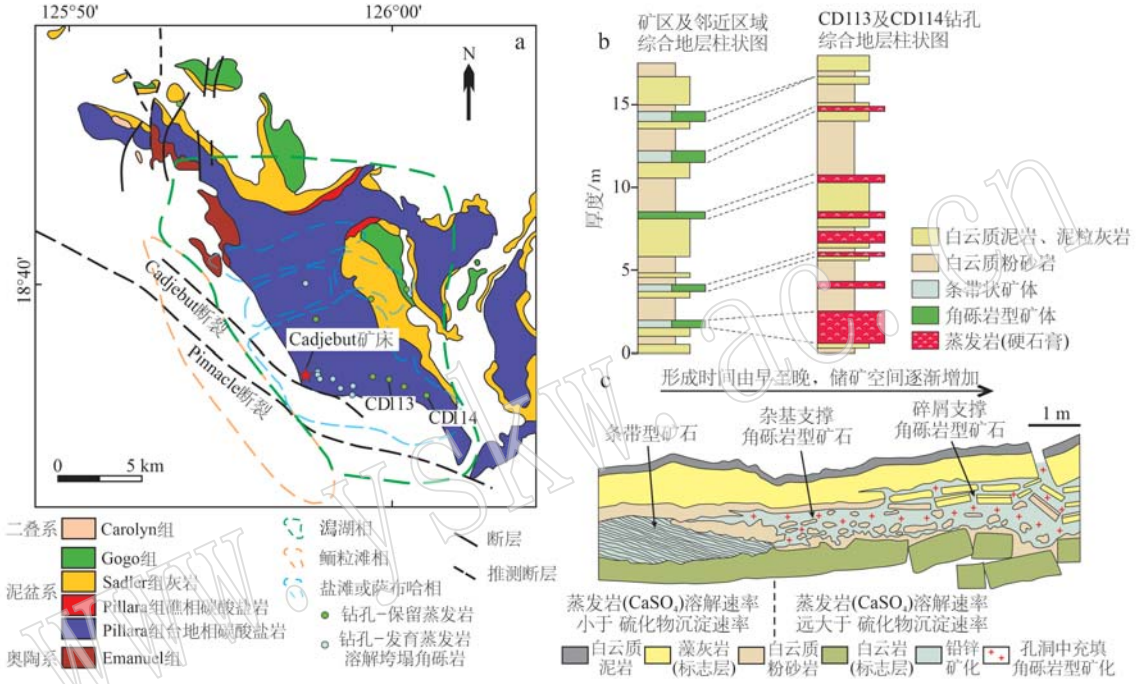

图 5　澳大利亚 Cadjebut 矿床与蒸发岩溶解垮塌构造

Fig. 5　Relationship between evaporite dissolution-collapse structure and Zn-Pb mineralization in the Cadjebut deposit, Australia

a—区域地质及岩相古地理格局（据 Tompkins *et al.*，1994a；Warren，2016）；b—矿区与外围地层岩性柱状图（据 Warren and Kempton，1997；Warren，2016）；c—蒸发岩溶解垮塌构造与不同类型矿化特征（据 Warren and Kempton，1997 修改）

a—geological map of the Cadjebut deposit with sedimentary facies of the Devonian host rocks (Tompkins *et al.*, 1994a; Warren, 2016); b—comparison between stratigraphic columns of the deposit area and its adjacent areas (Warren and Kempton, 1997; Warren, 2016); c—schematic diagram showing ore distribution in evaporite dissolution-collapse structure (modified from Warren and Kempton, 1997)

我国茂租矿床（矿石 17.5 Mt，Pb+Zn 品位 11.4%）位于扬子板块西南缘的川-滇-黔 MVT 铅锌矿集区内，赋矿地层为新元古代末震旦系灯影组上段白云岩，该时期区域上整体以浅海碳酸盐台地相为主，包括潮坪相、台缘及台内丘滩相、潟湖相（邹才能等，2014；刘静江等，2015；单秀琴等，2016）。矿床赋矿围岩为潮坪相沉积环境，矿体常就位于潮坪相各沉积旋回顶部的富蒸发岩潮上坪或萨布哈亚相白云岩中（图 6a，Tian *et al.*，2022）。赋矿层位分上、下两段，以上段为主，由上自下的白云岩中分别发育角砾岩、斑马构造、鸟眼构造（图 6a~6c）。铅锌矿体主要呈层状、似层状及透镜状产出，以角砾岩型和纹层状矿石为主（图 6d、6e）。角砾岩体侧向上断续出现，单个角砾岩体侧向延伸几米到十几米，垂向上几十厘米到几米。角砾为白云岩，呈棱角状且大小不一，有的角砾长轴方向近平行于地层，可见角砾相对地层方向呈向下垮塌的特征（图 6d），角砾岩体内未见明显内沉积。角砾杂基发生强烈的硅化和白云石化，可见白云石和石英的板柱状硬石膏假晶（图 7a、7b）。结合角砾岩特征和赋矿建造沉积相，推测角砾岩为蒸发岩溶解垮塌角砾岩。角砾间杂基经历白云石化和硅化作用，形成大量晶间孔，闪锌矿、方

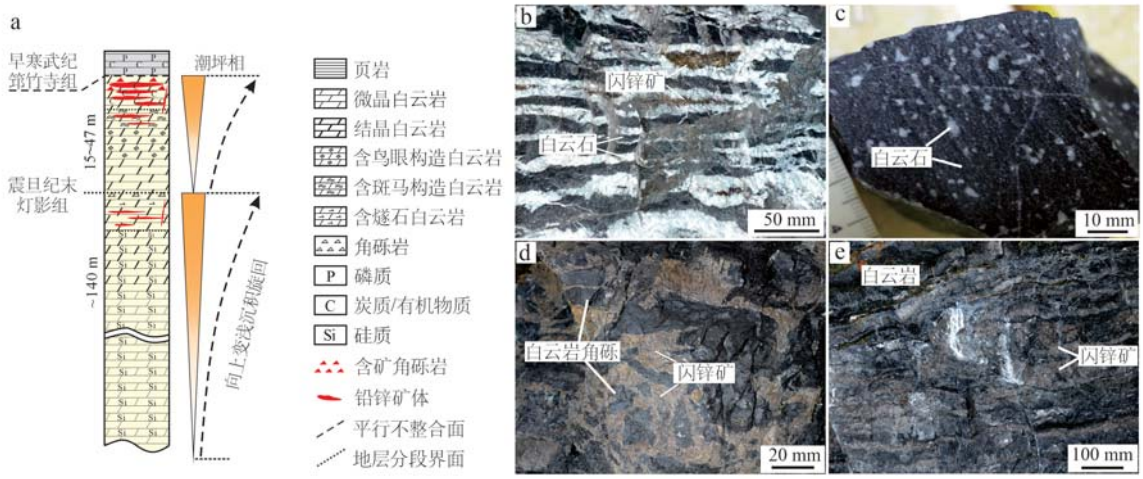

图 6 扬子西南缘茂租铅锌矿床与蒸发岩溶解垮塌构造

Fig. 6 Relationship between evaporite dissolution-collapse structure and Zn-Pb mineralization in the Maozu deposit, southwestern Yangtze

a—矿床综合岩性柱状图及对应沉积旋回(据 Tian *et al.*, 2022); b—含斑马构造白云岩; c—含鸟眼构造白云岩; d—角砾岩型矿石, 白云岩角砾间杂基中发育闪锌矿; e—纹层状矿石

a—stratigraphic columns of Maozu deposit, showing the sedimentary cycle (from Tian *et al.*, 2022); b—dolostone with zebra texture (specimen); c—dolostone with bird's eye texture; d—brecciaed ore, with sphalerite developed in the matrix of breccias; e—laminated ore, with sphalerite interbedded with dolomite band

铅矿充填-交代晶间孔隙(Tian *et al.*, 2022)(图 7c)。纹层状矿化出现在相对完整的白云岩中,白云岩经历白云石化形成顺层的晶间孔,铅锌硫化物充填-交代其中(图 7d)。此外,广泛发育的压溶缝、斑马构造、微裂缝中也充填少量铅锌硫化物。

Gays River(矿石 2.4 Mt,Pb+Zn 品位 14.9%)和 Jubilee 矿床(矿石 0.9 Mt, Pb+Zn 品位 6.6%)位于加拿大中东部 Maritimes 蒸发盆地边缘(Kontak and Jackson, 1995; Fallara and Savard, 1998; Sangster *et al.*, 1998)。矿床赋矿围岩为石炭系 Windsor 群底部 Gays River 组和 Macumber 组碳酸盐岩(Savard, 1996; Lynch *et al.*, 1998),两个组均具有向上变浅的浅滩相沉积特征(Boehner, 1989),上覆地层为石膏、硬石膏、岩盐等组成的海相蒸发岩(图 8a, Giles, 1981)。铅锌矿体主要分布在碳酸盐岩顶部与蒸发岩的接触带(图 8b, Akande and Zentilli, 1984; Kontak *et al.*, 1994),以块状和浸染状矿石为主,硬石膏在矿化部位较为常见(McKee *et al.*, 1985; Warren, 2016),浸染状矿化见于白云岩中。可见角砾岩型矿石,角砾为灰岩,直径约 2 ~ 30 mm,呈棱角状,角砾间为硫化物和方解石矿物胶结,推测为蒸发岩溶解垮塌成因。同层位的 Jubilee 矿床以角砾岩型矿化为主,含矿角砾岩体在碳酸盐岩层顶部顺层发育,与下伏岩性段呈突变接触,部分角砾岩显示为碎屑支撑,角砾达厘米级,呈棱角-次棱角状无序分布,具有蒸发岩溶解垮塌角砾岩特征(Chi *et al.*, 1995; Fallara and Savard, 1998; Lavoie *et al.*, 1998; Warren, 2000)。硫化物以细-中晶粒状闪锌矿、方铅矿为主,充填于溶蚀孔、晶间孔等开放空间以及角砾岩胶结物中(Akande and Zentilli, 1984; Savard, 1996; Fallara and Savard, 1998; Warren, 2016)。

4.2 盐底辟构造

4.2.1 基本特征及识别标志

蒸发岩具有低密度、不可压缩性及屈服强度小等属性,在重力、浮力、热对流及区域构造应力作用下,易发生流变导致岩层变形,形成盐构造(salt tectonics/halotectonics; 戈红星等, 1996; Hudec and Jackson, 2006, 2007; Warren, 2016; Jackson and Hudec, 2017),当蒸发岩充足时,可发生向上穿刺,形成底辟构造(Edgell, 1996; Hudec and Jackson, 2007)。盐底辟过程中会产生断层、裂缝,为地下流体运移提供通道(Demaison and Huizinga, 1991),底辟体顶部往往形成穹隆构造,有利于流体汇聚,同时厚层蒸发岩也相对致密,具有低渗透率特征,成为封闭性好的流体盖层,因此盐底辟构造是重要的储油构造(贾承造等, 2003; Volozh *et al.*, 2003; Hudec and

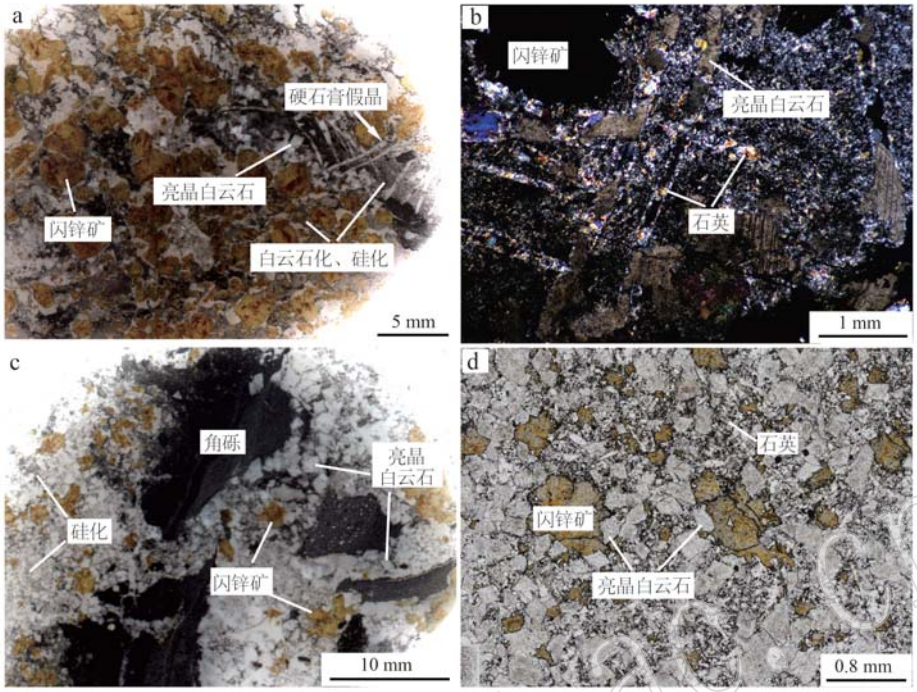

图 7　茂租矿床含矿岩石及铅锌矿化特征

Fig. 7　The host rocks and associated Zn-Pb sulfide mineralization in the Maozu deposit

a—含矿角砾岩杂基中发育板柱状硬石膏假晶；b—含矿角砾岩杂基中发育的硬石膏假晶被石英和白云石交代和充填（正交偏光）；c—含矿角砾岩杂基中白云石晶间孔被闪锌矿充填和交代；d—纹层状矿石中，闪锌矿出现在白云石晶间孔隙中（单偏光）

a—ore-hosting breccias containing tabular pseudomorphs after anhydrite in matrix; b—filling and replacement of tabular pseudomorphs after anhydrite by quartz and dolomite in the ore-hosting breccias (cross-polarized light); c—sphalerite filling and replacing the intercrystalline pores between crystalline dolomite and quartz in the breccia matrix; d—sphalerite filling and replacing the intercrystalline pores between crystalline dolomite in stratiform ores (plane-polarized light)

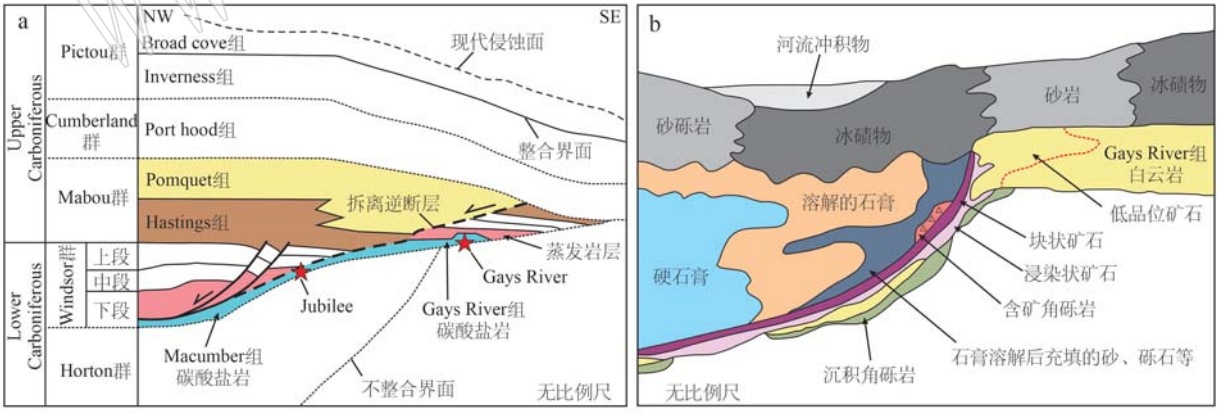

图 8　加拿大 Gays River 和 Jubilee 矿床区域地层剖面示意图（a，据 Savard，1996；Lynch *et al.*，1998；Warren，2000）和 Gays River 矿床蒸发岩与矿体关系剖面示意图（b，据 Akande and Zentilli，1984；Kontak *et al.*，1994；Warren，2016 修改）

Fig. 8　Schematic cross-section of regional stratigraphy at the Gays River -Jubilee region, Canada (a, from Savard, 1996; Lynch *et al.*, 1998; Warren, 2000) and schematic cross-section at Gays River showing Zn-Pb sulfide mineralization in evaporite dissolutioncollapse structure (b, modified from Akande and Zentilli, 1984; Kontak *et al.*, 1994; Warren, 2016)

Jackson，2007；Fetter，2009；余一欣等，2011；Michael *et al.*，2014）。

蒸发岩底辟体形态复杂多样，可直立状或倾斜状（Hudec and Jackson，2007），垂向延伸可超 10 km（Bouhlel *et al.*，2016）。在盐底辟过程中，底辟体两侧及顶部岩层内常伴生断层和裂隙，在底辟体边缘

形成黏土鞘,可使两侧地层形成沉积坳陷并堆积较厚沉积物,构成边缘向斜(图 9,Laznicka, 1988)。随着不断埋深,在其顶部的石膏和硬石膏发生碳酸盐化,形成冠岩(caprock)(图 9, Posey and Kyle, 1988; Kyle and Posey, 1991; Jaworska, 2010)。在墨西哥湾盆地,冠岩厚度一般为 100 ~ 150 m,最厚处可超过 300 m,两侧则相对较薄(Hallager *et al.*, 1990; Warren, 2016)。蒸发岩在向上底辟过程中会破碎围岩地层,在底辟体内部形成盐底辟角砾岩(Hearon *et al.*, 2014)。此类角砾岩常跨层产出,显示非角砾支撑特点,砾石大小不一,呈棱角-次棱角状,杂基中可见具有明显流动特征的蒸发岩(Sheppard *et al.*, 1996; Leach *et al.*, 2017)。蒸发岩可以底辟出地表,与地表沉积物混合,形成盐冰川(evaporite glaciers; Hudec and Jackson, 2006, 2007)。蒸发岩底辟构造顶部,也常伴有溶解垮塌形成的角砾岩(图 9, Laznicka, 1988; Warren, 2016)。

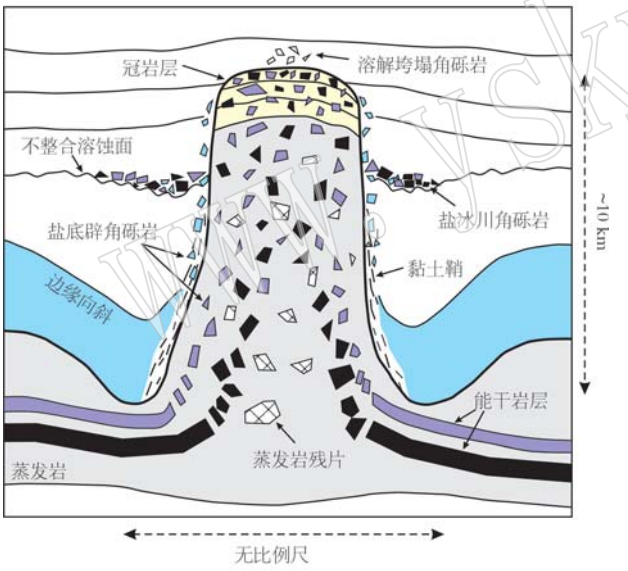

图 9 墨西哥湾典型盐底辟构造模型(据 Warren, 2016; Leach *et al.*, 2017 修改)

Fig. 9 Model of salt diapiric structure in the Gulf of Mexico (modified from Warren, 2016; Leach *et al.*, 2017)

在盐底辟、尤其是在古老盐底辟构造中,蒸发盐矿物常常“消失”,常常仅保留具有构造轮廓的角砾岩体,角砾岩本身常被误认为是挤压或断裂构造、水压致裂、溶解垮塌等成因(Ollier, 2007)。盐底辟角砾岩的特征可归纳为:① 角砾岩体在空间上穿切不同地层,垂向上延伸较远而侧向延伸相对有限;② 角砾岩砾石成分复杂,可来自当前部位下部的岩石,角砾呈棱角状无序分布,直径变化大(厘米至百米级),常具杂基支撑特点;③ 角砾岩杂基中可能发育蒸发盐矿物假晶、硬石膏残留、变质蒸发盐矿物(如钠长石、方柱石)等(Warren, 2016; Leach and Song, 2019; Zhuang *et al.*, 2023)。

在北非突尼斯和摩洛哥(Bouhlel *et al.*, 2007, 2009, 2016; Bouabdellah *et al.*, 2014, 2015; Rddad *et al.*, 2019)、欧洲南部西班牙(Rouvier *et al.*, 1985; Perona *et al.*, 2018)、北美墨西哥湾(Kyle and Posey, 1991; Kyle and Saunders, 1996)均发育大量盐底辟体,一些 MVT 矿床受控于这些盐底辟构造,但矿床规模较小。相比较,中国、伊朗和秘鲁境内与盐底辟构造相关的几个 MVT 矿床规模较大(Leach *et al.*, 2017; de Oliveira, 2019; Leach and Song, 2019; Song *et al.*, 2020; Zhuang *et al.*, 2023)。

4.2.2 矿床实例

在盐底辟构造有关的 MVT 铅锌矿床中,矿体与盐底辟构造的空间关系可分为 4 种情况:铅锌矿化① 赋存于直立底辟体顶部冠岩层和边部,如北美墨西哥湾盐构造带内一些矿床;② 位于盐底辟体紧邻的围岩地层内,如北非突尼斯 Bou Jabeur, Bou Grine, Slata, Fedj el Adoum 等矿床;③ 位于直立的盐底辟角砾筒内,如伊朗 Angouran 矿床、我国大梁子和天宝山矿床;④ 位于侧向底辟形成的盐穹隆体顶部,如我国金顶矿床。

北美墨西哥湾地区发育 Hockley、Winnfield 和 Tatum 等一系列近直立的盐底辟体,系在伸展背景下由侏罗系蒸发岩底辟而成。底辟体主要由硬石膏组成,富含岩石角砾,底辟体直径可达 4.4 km,最大延伸高度超 5 km(Price and Kyle, 1983; Kyle and Posey, 1991)。底辟体的顶部经历了油气流体的聚集,其与硬石膏相互作用(TSR 或 BSR),形成了方解石和 H_2S,这些富方解石的部位称为冠岩,除方解石外,还含硬石膏、石膏及岩石角砾(图 10a)。铅锌矿化出现在冠岩内,也出现底辟体边部,硫化物有闪锌矿、方铅矿、黄铁矿、白铁矿等。铅锌硫化物呈条带状、纹层状、不规则脉状交代方解石,也充填于方解石及硬石膏溶解的残留孔洞中,并可见天青石、重晶石等其他硫酸盐矿物(Ulrich *et al.*, 1984; Kyle and Price, 1986; Kyle and Agee, 1988; Kyle, 1991; Kyle and Posey, 1991)。

在北非突尼斯,区域挤压使三叠系蒸发岩发生底辟形成盐底辟构造(Perthuisot, 1981),底辟体直径

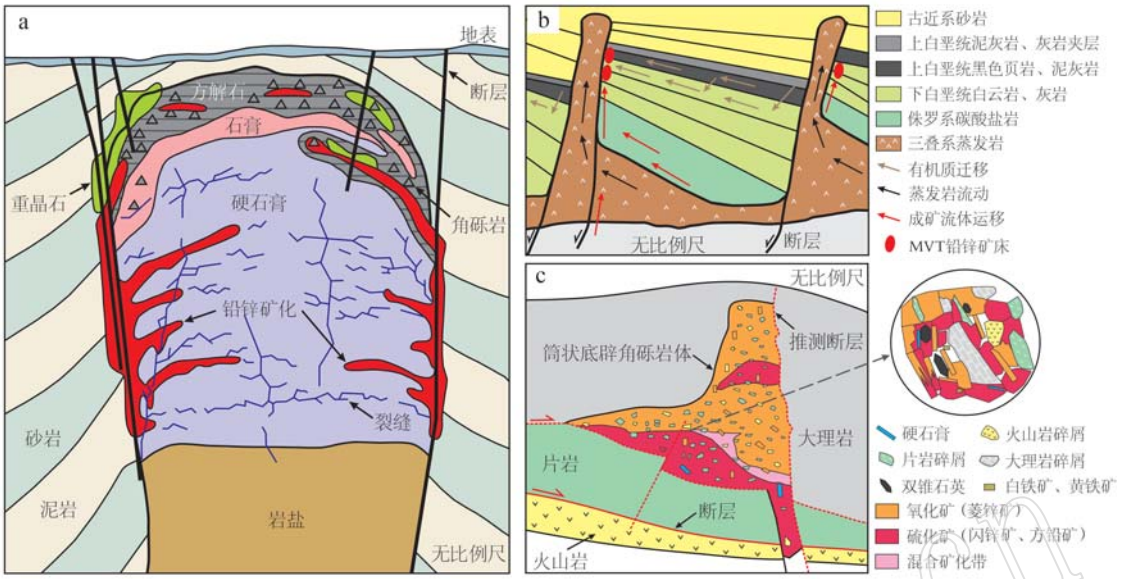

图 10　盐底劈构造控矿模型示意图

Fig. 10　Schematic diagram of ore-controlling models in salt diapiric structure

a—北美墨西哥湾盐底辟体与铅锌矿化关系模式图，铅锌矿化主要出现在底辟体顶部和边部（据 Kyle, 1991; Kyle and Posey, 1991; Warren, 2016 修改）；b—北非突尼斯 Slata 矿床盐底辟体，铅锌矿化出现邻近底辟体的碳酸盐岩中（据 Rddad *et al.*, 2019）；c—伊朗 Angouran 矿床盐底辟角砾岩筒，整个角砾岩筒发生原生硫化物矿化，后来上部发生表生氧化（据 Zhuang *et al.*, 2023）

a—schematic diagram showing the relationship between evaporite diapirs and Zn-Pb sulfide mineralization in the Gulf of Mexico, North America, where ores occur mainly in the caprock and margins of diapirs (modified from Kyle, 1991; Kyle and Posey, 1991; Warren, 2016); b—zinc and lead sulfide mineralization occurring in the peridiapiric carbonates of the Slata deposit, Tunisia, North Africa (Rddad *et al.*, 2019); c—zinc and lead sulfide mineralization hosted by evaporite diapir breccia pipe in Angouran deposit, Iran, the upper part of the orebody was oxidized during supergene process (from Zhuang *et al.*, 2023)

约 1 ~ 2 km，延伸最大可达 30 km，以石膏、硬石膏为主，在水岩相互作用和膏盐溶解作用下，底辟体与上覆及旁侧碳酸盐岩地层间发育以碎裂或镶嵌状角砾岩为主的“过渡带”（Bouhlel *et al.*, 2007, 2016）。Bou Jabeur（矿石 8 Mt，Pb+Zn 品位 5% ~ 15%）、Bou Grine（矿石 7.3 Mt，Pb + Zn 品位 12%）、Fedj el Adoum（矿石 1.5 Mt，Zn+Pb 品位 17% ）、Slata（矿石 0.16 Mt，Zn+Pb 品位 2.5%）等铅锌矿床赋存于底辟体边部的“过渡带”和邻近底辟体的白垩系碳酸盐岩层内（图 10b），闪锌矿、方铅矿、黄铁矿等硫化物出现在角砾岩及溶蚀孔洞中，或直接发育在底辟体伴生的断裂构造及不整合界面处（Bouhlel *et al.*, 2007, 2009, 2016; Rddad *et al.*, 2019）。铅锌矿化与富含有机质地层关系密切（Soua, 2009; Rddad *et al.*, 2019），有机质为硫酸盐还原过程提供充足还原剂，而盐底辟体提供硫和作为限制流体流动的物理屏障，二者共同导致成矿流体汇聚成矿（Sheppard *et al.*, 1996; Jemmali *et al.*, 2011; Bouhlel *et al.*, 2016）。

伊朗 Angouran 超大型 MVT 铅锌矿床（矿石 19.3 Mt, Zn+Pb 品位 27.4%）赋存于新元古界-寒武系大理岩-片岩建造中的一个直立角砾岩筒内（图 10c），大理岩-片岩建造逆冲在中新世含蒸发岩和火山岩的地层之上。角砾筒主体在大理岩中，直径约 200 ~ 400 m，向下延伸超 200 m（Gilg *et al.*, 2006; Boni *et al.*, 2007; Daliran *et al.*, 2013）。角砾岩中角砾主要由围岩的大理岩和片岩组成，少量有来自角砾岩筒下方的中新世火山岩。角砾直径从几厘米至数十米不等，分选较差，呈棱角状，可见悬浮角砾岩，具有明显杂基支撑的特征（图 11a），也见少量镶嵌状角砾岩（图 11b），有时角砾边缘的杂基具有流动构造（图 11）。角砾间杂基中除铅锌矿化外，可见大量硬石膏假晶（图 11c），在闪锌矿中发现有硬石膏包裹体并被闪锌矿所交代（图 11d）；同时，杂基中见双锥状石英（图 2d），具有高的 K 和 B 含量，与蒸发岩环境产出的双锥状石英特点一致。角砾岩筒的上述特征难以用岩溶垮塌和水压制裂来解释，无高温热液蚀变特点也难以用热液隐爆作用解释，因此

推断为盐底辟成因(Zhuang *et al.*, 2023)。铅锌矿化出现整个角砾岩筒内,上部以表生成因的菱锌矿化为主,下部以原生铅锌硫化物矿化为主,二者之间为两类矿化的混合(图 10c)。研究推测,在上新世区域挤压逆冲背景下,大理岩-片岩等基底岩石逆冲到中新世富蒸发盐的火山岩建造之上,同时诱发盆地中的蒸发盐发生底辟作用(Zhuang *et al.*, 2023)。在 Angouran 矿床,盐底辟作用导致大理岩和片岩发生破碎,形成盐底辟角砾岩筒,随后的硫化物铅锌矿化作用及后来表生作用使角砾岩中蒸发岩几乎完全溶解流失。我国川西大梁子(矿石 40 Mt,Zn+Pb 品位 11.3%)和天宝山(矿石 24.4 Mt, 品位 Zn+Pb 10.6%)矿床均产于角砾岩筒内(Zhou *et al.*, 2013; 袁波等, 2014),推测为盐底辟成因,但角砾岩筒中的蒸发岩在成矿前可能发生了强烈的溶解,导致上覆岩石垮塌而陷落到角砾岩筒内(Leach and Song, 2019)。

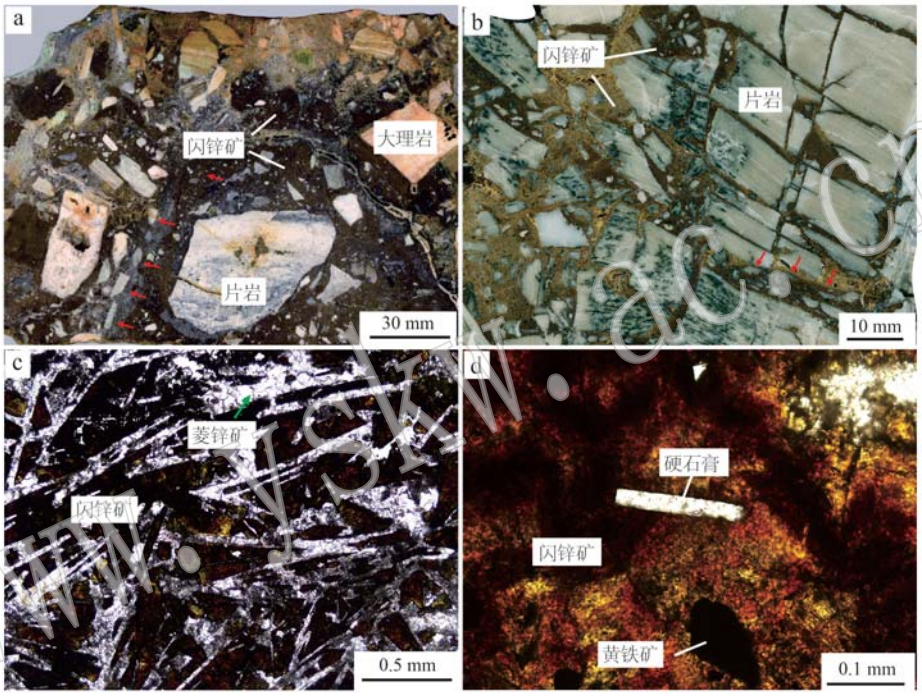

图 11 伊朗 Angouran 矿床角砾岩及铅锌矿化(Zhuang *et al.*, 2023)

Fig. 11 Breccias and associated Zn-Pb mineralization in the Angouran deposit, Iran (Zhuang *et al.*, 2023)

a—片岩和大理岩角砾被闪锌矿胶结,角砾呈棱角状,杂基支撑,局部可见流动构造(红色箭头); b—闪锌矿胶结棱角状片岩角砾,具镶嵌结构,局部呈悬浮结构(红色箭头); c—闪锌矿被菱锌矿交代,两者呈硬石膏矿物假晶(单偏光); d—闪锌矿中见自形板柱状硬石膏包体(单偏光)

a—angular clasts of schist and marble cemented by sphalerite showing a matrix-supported and flow-textured breccia, the flow texture is characterized by preferentially oriented rock fragments surrounding a larger marble clast (red arrows); b—mosaic clasts of angular schist cemented by sphalerite with locally floated texture (red arrows); c—sphalerite and smithsonite pseudomorphs after anhydrite, where sphalerite has been partially or totally replaced by smithsonite (plane-polarized light); d—rectangular anhydrite inclusion in sphalerite (plane-polarized light)

金顶超大型 MVT 铅锌矿床(矿石 200 Mt, Zn+Pb 品位 7.4%)位于我国滇西兰坪盆地内(Xue *et al.*, 2007)。矿床地层构成穹隆构造, Song 等(2020)将相关岩石划分为上、中、下 3 个构造单元,主要是中部单元赋矿(图 12a、12b),包括:(Ⅰ)与上、下构造单元呈断层接触的大规模灰岩角砾岩(图 13a),角砾呈棱角状,粒径厘米至数十米不等,胶结物由方解石、石膏/硬石膏、细小灰岩组成,含大量具有流动及穿刺特征的石膏和硬石膏体(图 13b、13c),为底辟成因角砾岩;(Ⅱ)与灰岩角砾岩体呈侧向过渡、具沉积构造的含灰岩角砾砂岩(图 13d),角砾呈棱角状,杂基中可见石膏,为底辟过程中膏盐体与原地沉积砂岩混合再沉积形成;(Ⅲ和Ⅳ)与上、下地层单元呈断层接触的膏-砂混杂体和砂体,前者胶结物中可见石膏,常被方解石、黄铁矿/白铁矿交代,后者砂体为硫化物和方解石组成的杂基支撑,底部可见具有明显流动及穿刺特征石膏,为膏-砂底辟相岩石。铅锌硫化物包括闪锌矿、方铅矿、黄铁矿、白

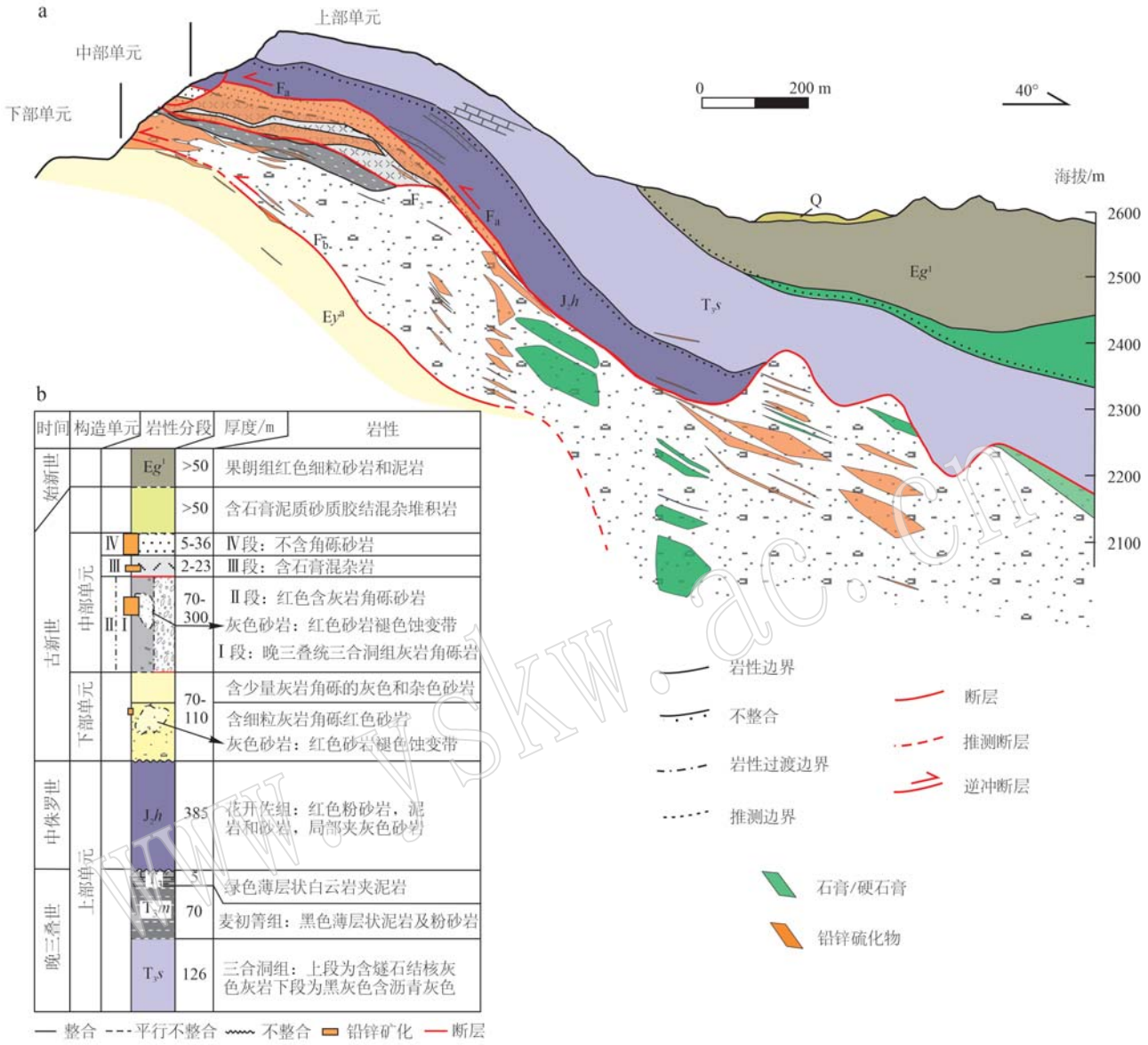

图 12　金顶矿床盐底辟穹隆构造与铅锌矿化关系剖面图（a）和地层柱状图（b）（据 Song *et al.*，2020；Huang *et al.*，2024 修改）

Fig. 12　Cross section showing lead and zinc sulfide mineralization in the dome created by lateral evaporite diapirism (a) and stratigraphic column of the Jinding deposit (b) (modified from Song *et al.*, 2020; Huang *et al.*, 2024)

铁矿等，其交代砂岩和灰岩角砾岩中的方解石等胶结物（图 13e），或充填于方解石晶洞中呈胶状结构生长（图 13f）。此外，矿区内沥青和油气包裹体广泛发育，说明该穹隆为一个古油气藏，并可见砂岩与有机流体相互作用产生褪色现象，有机质与石膏和硬石膏相互作用形成碳同位素值较低的方解石，并伴随 H_2S 产生（黄世强，2019；Huang *et al.*，2024）。Leach 等（2017）和 Song 等（2020）等提出，在古新世挤压作用下，上三叠统三合洞组灰岩建造中的蒸发岩沿逆冲断层发生侧向底辟，并流出地表而形成相关岩石建造，进一步形成穹隆构造；随后，油气流体流入，与富蒸发岩围岩发生相互作用产生大量 H_2S；最后含铅锌盆地卤水注入，与还原硫发生混合沉淀出铅锌硫化物而成矿。

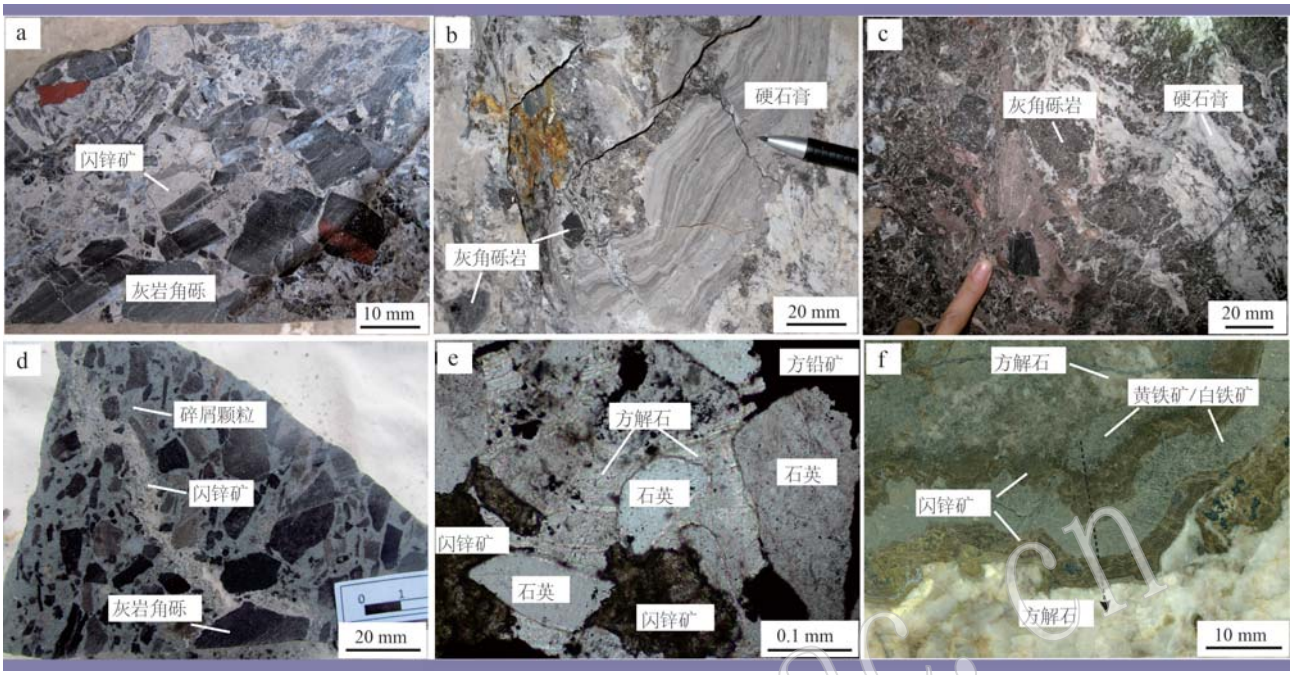

图 13 金顶矿床铅锌矿化特征

Fig. 13 Lead and zinc sulfide mineralization in the Jinding deposit

a—灰岩角砾岩,闪锌矿交代角砾间杂基; b—灰岩角砾岩中硬石膏,具有流动构造; c—灰岩角砾岩中硬石膏,"刺穿"灰岩围岩; d—含灰岩角砾砂岩,灰岩角砾呈棱角状,矿化发生在砂岩中; e—赋矿砂岩中石英颗粒间的方解石胶结物被闪锌矿、方铅矿等硫化物交代(单偏光); f—开放空间充填式矿化, 早期形成黄铁矿和方解石,随后胶状闪锌矿黄铁矿/白铁矿充填开放空间,最后形成粗晶方解石(箭头指向较晚沉淀的矿物)

a—sphalerite replacing matrix of brecciated limestones; b—flow-textured anhydrite in brecciated limestones; c—anhydrite of brecciated limestone injection into around limestone; d—angular limestone clasts in sandstone with Zn-Pb sulfide mineralization; e—calcite cement between quartz grains in sandstones replaced by sphalerite and galena (plane-polarized light); f—open-space filled style of mineralization showing as early calcite and pyrite precipitation, subsequent overgrowth of colloform sphalerite and pyrite/marcasite, and late formation of coarsely crystalline calcite (arrow denoting later minerals)

5 结语

蒸发岩与 MVT 铅锌矿床在成矿流体来源、硫来源及储矿构造等方面的关系紧密。其中,可有效迁移铅锌的盆地卤水主要来自蒸发海水,部分来自蒸发盐矿物的溶解,区域内蒸发岩的发育指示具有成矿流体形成条件。MVT 铅锌金属硫化物中的还原硫来自于硫酸盐的细菌还原或热化学还原作用,而地层中沉积的石膏和硬石膏等蒸发岩是硫酸盐的重要来源。蒸发岩溶解垮塌构造形成角砾岩与垮塌空间是铅锌矿化的主要部位,邻近的围岩也易发生矿化;与盐底辟构造有关矿床中铅锌矿化则赋存于底辟体顶部冠岩中、底辟体边部和邻近的围岩内、直立的盐底辟角砾筒中、以及侧向底辟形成的盐穹隆顶部。

蒸发盐矿物溶解或转变为其他矿物后,"消失"的蒸发岩较难识别。蒸发盐矿物的假晶和残留的蒸发盐矿物可作为蒸发岩曾经存在的证据,斑马、鸟眼、帐篷等结构构造、钠长石和方柱石等一些与蒸发岩有关的变质矿物、正延性玉髓/燧石、高碱土元素的双锥状石英等,均可能指示蒸发岩曾经发育。蒸发岩溶解垮塌和盐底辟构造独有的发育特征,可协助识别这两类构造。

区域发育蒸发岩(目前不一定得以完整保留)对于形成 MVT 铅锌矿床十分有利,甚至是必要条件。由于蒸发盐矿物容易"消失",准确识别蒸发岩及相关构造,十分重要。寻找 MVT 铅锌矿床,首先,需要评估区域是否出现过蒸发环境,比如地层中记录有蒸发岩或红层;其次,蒸发岩相关溶解垮塌和底辟构造是铅锌矿体定位的重要部位,是有利的找矿靶区,勘查过程中需要给予关注。

References

Akande S O and Zentilli M. 1984. Geologic, fluid inclusion, and stable isotope studies of the Gays River lead-zinc deposit, Nova Scotia Canada[J]. Economic Geology, 79: 1 187~1 211.

Anadón P, Rosell L and Talbot M R. 1992. Carbonate replacement of lacustrine gypsum deposits in two Neogene continental basins, eastern Spain[J]. Sedimentary Geology, 78(3~4): 201~216.

Anderson G M and Thom J. 2008. The role of thermochemical sulfate reduction in the origin of Mississippi Valley-type deposits. II. Carbonate-sulfide relationships[J]. Geofluids, 8: 27~34.

Beales F and Hardy J. 1977. The problem of recognition of occult evaporites with special reference to southeast Missouri[J]. Economic Geology, 72: 487~490.

Beales F W, Hardy J L, Zenger D H, *et al*. 1980. Criteria for the recognition of diverse dolomite types with an emphasis on studies on host rocks for Mississippi Valley-type ore deposits[C]//Concepts and Models of Dolomitization. SEPM Society for Sedimentary Geology, 28: 197~213.

Boehner R C. 1989. Carbonate buildups in the Lower Carboniferous Horton and Windsor groups (Late Tournaisian-Visean) of Nova Scotia [J]. Nova Scotia Department of Mines and Energy, 154~155.

Bouhlel S, Johnson C A and Leach D L. 2007. The peridiapiric-type Pb-Zn deposit at Fedj El Adoum, Tunisia: Geology, petrography, and stable isotopes[C]//Biennial SGA Meeting, 9th, Dublin, Ireland, Proceedings, 1: 323~326.

Bouhlel S, Leach D L, Johnson C A, *et al*. 2009. Ore textures and isotope signatures of the peridiapiric carbonate-hosted Pb-Zn deposit of Bougrine, Tunisia[C]//Biennial SGA Meeting, 10th, Townsville, Queensland, Proceedings, 1: 409~411.

Boni M, Gilg H A, Balassone G, *et al*. 2007. Hypogene Zn carbonate ores in the Angouran deposit, NW Iran[J]. Mineralium Deposita, 42(8): 799~820.

Bots P, Benning L G, Rickaby R E M, *et al*. 2011. The role of SO_4 in the switch from calcite to aragonite seas[J]. Geology, 39(4): 331~334.

Bouabdellah M, Castorina F, Bodnar R J, *et al*. 2014. Petroleum migration, fluid mixing, and halokinesis as the main ore-forming processes at the peridiapiric Jbel Tirremi fluorite-barite hydrothermal deposit, northeastern Morocco[J]. Economic Geology, 109(5): 1 223~1 256.

Bouabdellah M, Niedermann S and Velasco F. 2015. The Touissit-Bou Beker Mississippi Valley-type district of Northeastern Morocco: Relationships to the Messinian Salinity Crisis, Late Neogene-Quaternary alkaline magmatism, and Buoyancy-Driven fluid convection[J]. Economic Geology and the Bulletin of the Society of Economic Geologists, 110(6): 1 455~1 484.

Bouhlel S, Leach D L, Johnson C A, *et al*. 2016. A salt diapir-related Mississippi Valley-type deposit: The Bou Jaber Pb-Zn-Ba-F deposit, Tunisia: Fluid inclusion and isotope study[J]. Mineralium Deposita, 51(6): 749~780.

Bustillo M A, Armenteros I and Huerta P. 2017. Dolomitization, gypsum calcitization and silicification in carbonate-evaporite shallow lacustrine deposits[J]. Sedimentology, 64(4): 1 147~1 172.

Canfield D E. 2001. Isotope fractionation by natural populations of sulfate-reducing bacteria[J]. Geochimica et Cosmochimica Acta, 65(7): 1 117~1 124.

Canfield D E. 2004. The evolution of the Earth surface sulfur reservoir [J]. American Journal of Science, 304(10): 839~861.

Carpenter A B. 1978. Origin and chemical evolution of brines in sedimentary basins[J]. Oklahoma Geological Survey Circular, 79: 60~77.

Carlson E H. 1987. Celestite replacements of evaporites in the Salina Group[J]. Sedimentary Geology, 54(1~2): 93~112.

Caruso F, Alonge G, Bellia G, *et al*. 2017. Long-term monitoring of dolphin biosonar activity in deep pelagic waters of the Mediterranean Sea [J]. Scientific Reports, 7(1): 4 321.

Chambers L A and Trudinger P A. 1979. Microbiological fractionation of stable sulfur isotopes: A review and critique[J]. Geomicrobiology Journal, 1: 249~293.

Chen X Y, Chafetz H S, Andreasen R, *et al*. 2016. Silicon isotope compositions of euhedral authigenic quartz crystals: Implications for abiotic fractionation at surface temperatures[J]. Chemical Geology, 423: 61~73.

Chi G, Savard M M and Heroux Y. 1995. Constraints from fluid-inclusion data on the origin of the Jubilee carbonate-hosted Zn-Pb deposit, Cape Breton, Nova Scotia[J]. The Canadian Mineralogist, 33: 709~721.

Chi G X and Savard M M. 1997. Sources of basinal and Mississippi Valley-type mineralizing brines: Mixing of evaporated seawater and halite-dissolution brine[J]. Chemical Geology, 143(3~4): 121~125.

Claypool G E, Holser W T, Kaplan I R, *et al*. 1980. The age curves of sulfur and oxygen isotopes in marine sulfate and their mutual interpretation[J]. Chemical Geology, 28: 199~260.

Daley B. 1989. Silica pseudomorphs from the Bembridge Limestone (Upper Eocene) of the Isle of Wight, Southern England and their palaeoclimatic significance [J]. Palaeogeography, Palaeoclimatology, Palaeoecology, 69: 233~240.

Daliran F, Pride K, Walther J, *et al*. 2013. The Angouran Zn (Pb) deposit, NW Iran: Evidence for a two stage, hypogene zinc sulfide-zinc carbonate mineralization[J]. Ore Geology Reviews, 53: 373~402.

de Oliveira S B, Leach D L, Juliani C, *et al*. 2019. The Zn-Pb mineralization of Florida Canyon, an evaporite-related Mississippi Valley-type deposit in the Bongará District, Northern Peru[J]. Economic Geology, 114: 1 621~1 647.

Demaison G and Huizinga B J. 1991. Genetic classification of petroleum systems[J]. AAPG Bulletin, 75: 1 626~1 643.

Detmers J, Brüchert V, Habicht K S, *et al*. 2001. Diversity of sulfur isotope fractionations by sulfate-reducing prokaryotes[J]. Applied and Environmental Microbiology, 67(2): 888~894.

Dill H G, Henjes-Kunst F, Berner Z, *et al*. 2009. Miocene diagenetic and epigenetic strontium mineralization in calcareous series from Cyprus and the Arabian Gulf: Metallogenic perspective on sub- and suprasalt redox-controlled base metal deposits[J]. Journal of Asian Earth Sciences, 34(4): 557~576.

Edgell H S. 1996. Salt tectonism in the Persian Gulf Basin[J]. Geological Society of London Special Publications, 100(1): 129~151.

Emsbo P, Hagemann S G and Brown P E. 2000. Gold in Sedex deposit [J]. Society of Economic Geologist, 427~437.

Fallara F and Savard M M. 1998. A structural, petrographic, and geochemical study of the Jubilee Zn-Pb deposit, Nova Scotia, Canada, and a new metallogenic model[J]. Economic Geology, 93: 757~778.

Fernández-Díaz L, Fernández-González Á and Prieto M. 2010. The role of sulfate groups in controlling $CaCO_3$ polymorphism[J]. Geochimica et Cosmochimica Acta, 74(21): 6 064~6 076.

Fernández-Díaz L, Pina C M, Astilleros J M, *et al*. 2009. The carbonatation of gypsum: Pathways and pseudomorph formation[J]. American Mineralogist, 94: 1 223~1 234.

Fetter M. 2009. The role of basement tectonic reactivation on the structural evolution of Campos Basin, offshore Brazil: Evidence from 3D seismic analysis and section restoration[J]. Marine and Petroleum Geology, 26(6): 873~886.

Folk R L and Pittman J S. 1971. Length-slow chalcedony: A new testament for vanished evaporites[J]. Journal of Sedimentary Research, 41: 1 045~1 058.

Ford D C and Williams P. 2007. Karst Hydrogeology and Geomorphology [M]. Chichester: John Wiley & Sons.

Friedman G M. 1997. Dissolution-collapse breccias and paleokarst resulting from dissolution of evaporite rocks, especially sulfates[J]. Carbonates and Evaporites, 12: 53~63.

Friedman G M and Shukla V. 1980. Significance of authigenic quartz euhedra after sulfates; example from the Lockport Formation (Middle Silurian) of New York[J]. Journal of Sedimentary Research, 50: 1 299~1 304.

Gandin A, Wright D T and Melezhik V. 2005. Vanished evaporites and carbonate formation in the Neoarchaean Kogelbeen and Gamohaan formations of the Campbellrand Subgroup, South Africa[J]. Journal of African Earth Sciences, 41(1~2): 1~23.

Ge Hongxing and Jackson M P A. 1996. Salt structures, hydrocarbon traps and mineral deposits[J]. Journal of Nanjing University (Natural Sciences), 32(4): 640~649 (in Chinese with English abstract).

Giles P S. 1981. Major transgressive-regressive cycles in middle to late Visean rocks of Nova Scotia[J]. Nova Scotia Department of Mines and Energy, 81-2: 1~27.

Gilg H A, Boni M, Balassone G, *et al*. 2006. Marble-hosted sulfide ores in the Angouran Zn-(Pb-Ag) deposit, NW Iran: Interaction of sedimentary brines with a metamorphic core complex[J]. Mineralium Deposita, 41(1): 1~16.

Goldhaber M B and Kaplan I R. 1975. Controls and consequences of sulfate reduction rates in recent marine sediments[J]. Soil Science, 119(1): 42~55.

Götze J. 2012. Mineralogy, geochemistry and cathodoluminescence of authigenic quartz from different sedimentary rocks[J]. Quartz: Deposits, Mineralogy and Analytics, 287~306.

Grotzinger J P. 1986. Evolution of Early Proterozoic passive-margin carbonate platform, rocknest formation, wopmay orogen, Northwest Territories, Canada[J]. Journal of Sedimentary Research, 56(6): 831~847.

Hallager W S, Ulrich M R, Kyle J R, *et al*. 1990. Evidence for episodic basin dewatering in salt-dome cap rocks[J]. Geology, 18(8): 716.

Hanor J S. 1979. Geochemistry of Hydrothermal Ore Deposits[M]. New York: Wiley.

Hanor J S. 2000. Barite-Celestine geochemistry and environments of formation[J]. Reviews in Mineralogy & Geochemistry, 40: 193~275.

Hanor J S. 2004. A model for the origin of large carbonate- and evaporite-hosted celestine ($SrSO_4$) deposits[J]. Journal of Sedimentary Research, 74(2): 168~175.

Hearon T E, Rowan M G, Giles K A, *et al*. 2014. Halokinetic deformation adjacent to the deepwater Auger diapir, Garden Banks 470,

northern Gulf of Mexico: Testing the applicability of an outcrop-based model using subsurface data[J]. Interpretation, 2: SM57~SM76.

Henchiri M, Abidi R and Jemmali N. 2015. Large euhedral quartz crystals in the Triassic dolomites and evaporites of central Tunisia: Implications for silica diagenesis in sulphate-rich and high-Mg environments[J]. Arabian Journal of Geosciences, 8(10): 8 899~8 910.

Henchiri M and Slim-S'himi N. 2006. Silicification of sulphate evaporites and their carbonate replacements in Eocene marine sediments, Tunisia: Two diagenetic trends[J]. Sedimentology, 53: 1 135~1 159.

Hietanen A. 1967. On the facies series in various types of metamorphism [J]. The Journal of Geology, 75: 187~214.

Hitzman M W. 2000. Iron oxide-Cu-Au deposits: What, where, when and why[J]. Hydrothermal Iron Oxide Copper-Gold and Related Deposits, 9~25.

Huang G, Song Y C, Zhuang L L, *et al*. 2024. Genesis of celestine in the world-class Jinding Zn-Pb-Sr deposit, SW China: Constraints from field mapping, petrography, fluid inclusion, and elemental and S-O-Sr isotope geochemistry [J]. Ore Geology Reviews, 166: 105957.

Huang Shiqiang. 2019. Interaction Between Hydrocarbon Fluids and Host Rocks/Evaporites in the Jinding World-Class Zn-Pb Deposit: Implication for Ore Genesis[D]. Beijing: China University of Geosciences (in Chinese with English abstract).

Hudec M R and Jackson M P. 2006. Advance of allochthonous salt sheets in passive margins and orogens[J]. AAPG Bulletin, 90: 1 535~1 564.

Hudec M R and Jackson M P A. 2007. Terra infirma: Understanding salt tectonics[J]. Earth-Science Reviews, 82(1~2): 1~28.

Jackson M P A and Hudec M R. 2017. Salt Tectonics: Principles and Practice[M]. Cambridge University Press.

Jackson M P A, Warin O N, Woad G M, *et al*. 2003. Neoproterozoic allochthonous salt tectonics during the Lufilian orogeny in the Katangan Copperbelt, central Africa[J]. Geological Society of America Bulletin, 115: 314~330.

Jaworska J. 2010. An oxygen and sulfur isotopic study of gypsum from the Wapno Salt Dome cap-rock (Poland)[J]. Geological Quarterly, 54: 25~32.

Jemmali N, Souissi F, Vennemann T W, *et al*. 2011. Genesis of the Jurassic carbonate-hosted Pb-Zn deposits of Jebel Ressas (North-Eastern Tunisia): Evidence from mineralogy, petrography and trace metal contents and isotope (O, C, S, Pb) geochemistry[J]. Resource Geology, 61: 367~383.

Jia Chengzao, Zhao Wenzhi, Wei Guoqi, *et al*. 2003. Salt structures and exploration of oil and gas[J]. Petroleum Explorationand Development, 30(2): 17~19 (in Chinese with English abstract).

Jin Zhijun, Long Shengxiang, Zhou Yan, *et al*. 2006. A study on the distribution of saline-deposit in Southern China[J]. Oil & Gas Geology, 27(5): 571~583, 593 (in Chinese with English abstract).

Jin Zhijun, Zhou Yan, Yun Jinbiao, *et al*. 2010. Distribution of gypsum-salt cap rocks and near-term hydrocarbon exploration targets in the marine sequences of China[J]. Oil & Gas Geology, 31(6): 715~724 (in Chinese with English abstract).

Jørgensen B B, Isaksen M F and Jannasch H W. 1992. Bacterial sulfate reduction above 100℃ in deep-sea hydrothermal vent sediments[J]. Science, 258: 1 756~1 757.

Keene J B. 1983. Chalcedonic quartz and occurrence of quartzine (length-slow chalcedony) in pelagic sediments[J]. Sedimentology, 30: 449~454.

Kendall A C. 1978. Facies models 12. subaqueous evaporites[J]. Geoscience Canada, 5(3): 124~139.

Kendall C G S C and Warren J. 1987. A review of the origin and setting of tepees and their associated fabrics[J]. Sedimentology, 34(6): 1 007~1 027.

Kesler S E, Martini A M, Appold M S, *et al*. 1996. Na-Cl-Br systematics of fluid inclusions from Mississippi Valley-type deposits, Appalachian Basin: Constraints on solute origin and migration paths[J]. Geochimica et Cosmochimica Acta, 60(2): 225~233.

Kesler S E and Reich M H. 2006. Precambrian Mississippi Valley-type deposits: Relation to changes in composition of the hydrosphere and atmosphere[J]. Acta Stomatologica Croatica, 185~204.

Kharaka Y K, Maest A S, Carothers W W, *et al*. 1987. Geochemistry of metal-rich brines from central Mississippi Salt Dome Basin, U. S. A [J]. Applied Geochemistry, 2(5~6): 543~561.

Kontak D J, Farrar E and Mcbride S L. 1994. $^{40}Ar/^{39}Ar$ dating of fluid migration in a Mississippi Valley-type deposit; the Gays River Zn-Pb deposit, Nova Scotia, Canada[J]. Economic Geology, 89(7): 1 501~1 517.

Kontak D J and Jackson S E. 1995. Laser-ablation ICP-MS micro-analysis of calcite cement from a Mississippi valley-type Zn-Pb deposit, Nova Scotia; dramatic variability in REE content on macro- and micro-scales[J]. The Canadian Mineralogist, 33(2): 445~467.

Krouse H R, Viau C A, Eliuk L S, *et al*. 1988. Chemical and isotopic evidence of thermochemical sulphate reduction by light hydrocarbon gases in deep carbonate reservoirs[J]. Nature, 333: 415~419.

Kyle J R. 1991. Evaporites, evaporitic processes and mineral resources [J]. Developments in Sedimentology, 50: 477~533.

Kyle J R and Agee W N. 1988. Evolution of metal ratios and $\delta^{34}S$ composition of sulfide mineralization during anhydrite cap rock formation, Hockley Dome, Texas, U.S.A[J]. Chemical Geology, 74(1~2): 37~55.

Kyle J R and Misi A. 1991. Origin of sulfide and phosphate deposits in Upper Proterozoic carbonate strata, Irece basin, Bahia, Brazil[J]. AAPG Bulletin, 75.

Kyle J R and Posey H H. 1991. Chapter 5 Halokinesis, Cap rock development, and salt dome mineral resources[J]. Evaporites Petroleum & Mineral Resources, 50: 413~474.

Kyle J R and Price P E. 1986. Metallic sulphide mineralization in salt-dome cap rocks, Gulf Coast, U.S.A[J]. Transactions of the Institution of Mining and Metallurgy. Section B. Applied Earth Science, 95: 6~16.

Kyle J R and Saunders J A. 1996. Metallic deposits of the Gulf Coast basin: Diverse mineralization styles in a young sedimentary basin[J]. International Conference on Carbonate-hosted Lead-Zinc Deposits, 4: 218~229.

Lavoie D, Sangster D F, Savard M M, *et al*. 1998. Breccias in the lower part of the Mississippian Windsor Group and their relation to Zn-Pb mineralization; a summary[J]. Economic Geology, 93: 734~745.

Laznicka P. 1988. Breccias and coarse fragmentites: Petrology, environments, associations, ores[J]. Developments in Economic Geology, 25.

Leach D L and Sangster D F. 1993. Mississippi Valley-type lead-zine deposits[J]. Geological Association of Canada-Special Paper, 40: 289~314.

Leach D L, Sangster D F, Kelley K D, *et al*. 2005. Sediment-hosted lead-zinc deposits: A global perspective[J]. Economic Geology, 100: 561~607.

Leach D L and Song Y. 2019. Sediment-hosted zinc-lead and copper deposits in China[C]//Chang Z and Goldfarb R J. Mineral Deposits of China. Society of Economic Geologists Special Publication, 22: 325~349.

Leach D L, Song Y C and Hou Z Q. 2017. The world-class Jinding Zn-Pb deposit: Ore formation in an evaporite dome, Lanping Basin, Yunnan, China[J]. Mineralium Deposita, 52(3): 281~296.

Lehmann K, Pettke T and Ramseyer K. 2011. Significance of trace elements in syntaxial quartz cement, Haushi Group sandstones, Sultanate of Oman[J]. Chemical Geology, 280(1~2): 47~57.

Leitner C, Wiesmaier S, Köster M H, *et al*. 2017. Alpine halite-mudstone-polyhalite tectonite: Sedimentology and early diagenesis of evaporites in an ancient rift setting (Haselgebirge Formation, eastern Alps)[J]. Geological Society of America Bulletin, 129: 1 537~1 553.

Liu Jiajun, Liu Zhenjiang, Yang Yan, *et al*. 2007. The salt roles in the mineralizing processes of metal and non-metal deposits[J]. Contributions to Geology and Mineral Resources Research, 22(3): 161~171 (in Chinese with English abstract).

Liu Jingjiang, Li Wei, Zhang Baomin, *et al*. 2015. Sedimentary palaeogeography of the Sinian in upper Yangtze Region[J]. Journal of Palaeogeography, 17(6): 735~753 (in Chinese with English abstract).

Lynch G, Keller J V A and Giles P S. 1998. Influence of the Ainslie Detachment on the stratigraphy of the Maritimes Basin and mineralization in the Windsor Group of northern Nova Scotia, Canada[J]. Economic Geology, 93: 703~718.

Machel H G. 2001. Bacterial and thermochemical sulfate reduction in diagenetic settings—Old and new insights[J]. Sedimentary geology, 140(1~2): 143~175.

Machel H G, Krouse H R and Sassen R. 1995. Products and distinguishing criteria of bacterial and thermochemical sulfate reduction[J]. Applied Geochemistry, 10(4): 373~389.

Maliva R G, Knoll A H and Simonson B M. 2005. Secular change in the Precambrian silica cycle: Insights from chert petrology[J]. Geological Society of America Bulletin, 117(7): 835.

McKee D M, Eng P, Hannon P J, *et al*. 1985. The hydrological environment at the Gays River mine[J]. International Journal of Mine Water, 4(2): 13~33.

Melezhik V A, Fallick A E, Rychanchik D V, *et al*. 2005. Palaeoproterozoic evaporites in Fennoscandia: Implications for seawater sulphate, the rise of atmospheric oxygen and local amplification of the $\delta^{13}C$ excursion[J]. Terra Nova, 17: 141~148.

Miall A D. 1985. Architectural-element analysis: A new method of facies analysis applied to fluvial deposits[J]. Earth-Science Reviews, 22(4): 261~308.

Michael C A, Dominey-Howes D and Labbate M. 2014. The antimicrobial resistance crisis: Causes, consequences, and management[J]. Frontiers in Public Health, 2: 145.

Moine B, Sauvan P and Jarousse J. 1981. Geochemistry of evaporite-bearing series: A tentative guide for the identification of metaevaporites[J]. Contributions to Mineralogy and Petrology, 76(4): 401~412.

Moldovanyi E P and Walter L M. 1992. Regional trends in water chemistry, Smackover Formation, southwest Arkansas: Geochemical and physical controls[J]. AAPG Bulletin, 76: 864~894.

Morrow D W. 1982. Descriptive field classification of sedimentary and diagenetic breccia fabrics in carbonate rocks[J]. Bulletin of Canadian Petroleum Geology, 30: 227~229.

Ohmoto H and Goldhaber B. 1997. Sulphur and carbon isotopes[J]. Geochemistry of Hydrothermal Ore Deposits, 1: 517~600.

Ollier C D. 2007. Breccia-filled pipes: Distinguishing between volcanic and non-volcanic origins[J]. Geografia Fisica e Dinamica Quaternaria, 30: 63~76.

Perkins R D, Dwyer G S, Rosoff D B, *et al*. 1994. Salina sedimentation and diagenesis: West Caicos Island, British West Indies[J]. Dolomites: A Volume in Honour of Dolomieu, 35~54.

Perona J, Canals À and Cardellach E. 2018. Zn-Pb Mineralization associated with salt diapirs in the Basque-Cantabrian Basin, northern Spain: Geology, geochemistry, and genetic model[J]. Economic Geology, 113(5): 1 133~1 159.

Perthuisot V. 1981. Diapirism in northern Tunisia[J]. Journal of Structural Geology, 3: 231~235.

Pierre C and Rouchy J M. 1988. Carbonate replacements after sulfate evaporites in the middle miocene of Egypt[J]. Journal of Sedimentary Research, 58: 446~456.

Posey H H and Kyle J R. 1988. Fluid-rock interactions in the salt dome environment: An introduction and review[J]. Chemical Geology, 74: 1~24.

Powell T G and MacQueen R W. 1984. Precipitation of sulfide ores and organic matter: Sulfate reactions at Pine Point, Canada[J]. Science, 224(4 644): 63~66.

Price P E and Kyle J R. 1983. Metallic sulfide deposits in Gulf Coast salt dome cap rocks[J]. AAPG Bulletin, 67: 1 470~1 470.

Rddad L, Jemmali N, Sonicka M, *et al*. 2019. The genesis of the salt diapir-related Mississippi Valley-type Ba-Pb-(± Zn) ore of the Slata district, Tunisia: The role of halokinesis, hydrocarbon migration, and alpine orogenesis[J]. Economic Geology, 114: 1 599~1 620.

Rittenhouse G. 1967. Bromine in oil-field waters and its use in determining possibilities of origin of these waters[J]. American Association of Petroleum Geologists Bulletin, 51(12): 2 430~2 440.

Roedder E. 1984. The fluids in salt[J]. American Mineralogist, 69: 413~439.

Rosa D, Leach D, Guarnieri P, *et al*. 2023. The Black Angel deposit, Greenland: A Paleoproterozoic evaporite-related Mississippi Valley-type Zn-Pb deposit[J]. Mineralium Deposita, 58(1): 51~73.

Rouvier H, Perthuisot V and Mansouri A. 1985. Pb-Zn deposits and salt-bearing diapirs in Southern Europe and North Africa[J]. Economic Geology, 80: 666~687.

Rusk B G, Lowers H A and Reed M H. 2008. Trace elements in hydrothermal quartz: Relationships to cathodoluminescent textures and insights into vein formation[J]. Geology, 36(7): 547~550.

Sangster D F. 1990. Mississippi Valley-type and sedex lead-zinc deposits: A comparative examination[J]. Trans. Inst. Mining and Metall., 99: 21~42.

Sangster D F, Savard M M and Kontak D J. 1998. A genetic model for mineralization of lower Windsor (Visean) carbonate rocks of Nova Scotia, Canada[J]. Economic Geology, 93: 932~952.

Sanz-Montero M E, Rodriguez-Aranda J P and Calvo J P. 2006. Mediation of endoevaporitic microbial communities in early replacement of gypsum by dolomite: A case study from Miocene Lake deposits of the Madrid Basin, Spain[J]. Journal of Sedimentary Research, 76(12): 1 257~1 266.

Sanz-Rubio E, Sánchez-Moral S, Cañaveras J C, *et al*. 2001. Calcitization of Mg-Ca carbonate and Ca sulphate deposits in a continental Tertiary Basin (Calatayud Basin, NE Spain)[J]. Sedimentary Geology, 140(1~2): 123~142.

Savard M M. 1996. Pre-ore burial dolomitization adjacent to the carbonate-hosted Gays River Zn-Pb deposit, Nova Scotia[J]. Canadian Journal of Earth Sciences, 33(2): 303~315.

Scholle P A, Stemmerik L and Harpoth O. 1990. Origin of major karst-associated celestite mineralization in Karstryggen, central East Greenland[J]. Journal of Sedimentary Research, 60: 397~410.

Seal R R. 2006. Sulfur isotope geochemistry of sulfide minerals[J]. Reviews in Mineralogy and Geochemistry, 61(1): 633~677.

Seal R R II and Wandless G A. 2003. Sulfur isotope evidence for sea-floor mineralizing processes at the Bald Mountain and Mount Chase massive sulfide deposits, northern Maine[J]. Econ. Geol. Monogr., 11: 567~587.

Shan Xiuqin, Zhang Jing, Zhang Baomin, *et al*. 2016. Dolomite karst reservoir characteristics and dissolution evidences of Sinian Dengying Formation, Sichuan Basin[J]. Acta Petrolei Sinica, 37(1): 17~29 (in Chinese with English abstract).

Sharma R S. 1981. Mineralogy of a scapolite-bearing rock from Rajasthan, northwest Peninsular India[J]. Lithos, 14(2): 165~172.

Sharp Z D. 2017. Principles of Stable Isotope Geochemistry, 2nd Edition[M]. New York: Pearson Education.

Sheppard S M F, Charef A, Bouhlel S, *et al*. 1996. Diapirs and Zn-Pb mineralization: A general model based on Tunisian (N. Africa) and Gulf Coast (U.S.A.) deposits[J]. Society of Economic Geologists Special Publication, 4: 230~243.

Siedlecka A. 1972. Length-slow chalcedony and relicts of sulphates; evi-

dences of evaporitic environments in the upper Carboniferous and Permian beds of Bear Island, Svalbard[J]. Journal of Sedimentary Research, 42: 812~816.

Smith D B. 1972. Foundered strata, collapse breccias and subsidence features of the English Zechstein[J]. Geology of Saline Deposits, 255~269.

Song Yucai, Hou Zengqian, Liu Yingchao, *et al*. 2017. Mississippi Valley-type (MVT) Pb-Zn deposits in the Tethyan domain: A review[J]. Geology in China, 44(4): 664~689 (in Chinese with English abstract).

Song Y C, Hou Z Q, Xue C D, *et al*. 2020. New mapping of the world-class Jinding Zn-Pb deposit, Lanping Basin, southwest China: Genesis of ore host rocks and records of hydrocarbon-rock interaction [J]. Economic Geology, 115(5): 981~1 002.

Soua M, Echihi O, Herkat M, *et al*. 2009. Structural context of the paleogeography of the Cenomanian-Turonian anoxic event in the eastern Atlas Basins of the Maghreb[J]. Comptes Rendus Geoscience, 341 (12): 1 029~1 037.

Spear F S. 1993. Metamorphic phase equilibria and pressure-temperature-time paths[J]. Mineralogical Society of America, 60(403): 992~993.

Sullivan L and Koppi A. 1993. Barite pseudomorphs after lenticular gypsum in a buried soil from central Australia[J]. Australian Journal of Soil Research, 31: 36~42.

Swennen R, Viaene W and Cornelissen C. 1990. Petrography and geochemistry of the Belle Roche breccia (lower Visean, Belgium): Evidence for brecciation by evaporite dissolution[J]. Sedimentology, 37: 859~878.

Taylor R D, Leach D L, Bradley D C, *et al*. 2009. Compilation of mineral resource data for Mississippi Valley-type and clastic-dominated sediment-hosted lead-zinc deposits[J]. Geological Survey Open-File Report, 1 297: 42.

Teboul P A, Durlet C, Girard J P, *et al*. 2019. Diversity and origin of quartz cements in continental carbonates: Example from the Lower Cretaceous Rift deposits of the South Atlantic margin[J]. Applied Geochemistry, 100: 22~41.

Thomas R J, Ellison R A, Goodenough K M, *et al*. 2015. Salt domes of the UAE and Oman: Probing eastern Arabia[J]. Precambrian Research, 256: 1~16.

Tian L D, Song Y C, Zhuang L L, *et al*. 2022. Characteristic and genesis of dolostone reservoirs around the Proterozoic/Cambrian boundary in the Upper Yangtze Block for Mississippi valley-type Zn-Pb ores: A review[J]. Ore Geology Reviews, 150: 105179.

Tompkins L A, Pedone V A, Roche M T, *et al*. 1994a. The Cadjebut Deposit as an example of mississippi valley-type mineralization on the Lennard Shelf, Western Australia; single episode or multiple events? [J]. Economic Geology, 89: 450~466.

Tompkins L A, Rayner M J, Groves D I, *et al*. 1994b. Evaporites; in situ sulfur source for rhythmically banded ore in the Cadjebut mississippi valley-type Zn-Pb deposit, Western Australia[J]. Economic Geology, 89: 467~492.

Trudinger P A, Chambers L A and Smith J W. 1985. Low-temperature sulphate reduction: Biological versus abiological[J]. Canadian Journal of Earth Sciences, 22: 1 910~1 918.

Tucker M E. 1976. Replaced evaporites from the late Precambrian of finnmark, Arctic Norway[J]. Sedimentary Geology, 16(3): 193~204.

Ulmer-Scholle D S, Scholle P A and Brady P V. 1993. Silicification of evaporites in Permian (Guadalupian) back-reef carbonates of the Delaware Basin, West Texas and New Mexico[J]. Journal of Sedimentary Research, 63: 955~965.

Ulrich M R, Kyle J R and Price P E. 1984. Metallic sulfide deposits in Winnefield salt dome, Louisiana: Evidence for episodic introduction of metalliferous brines during cap rock formation[J]. AAPG Bulletin, 68(9): 435~442.

Velasco F, Herrero J M, Yusta I, *et al*. 2003. Geology and geochemistry of the Reocin zinc-lead deposit, Basque-Cantabrian Basin, Northern Spain[J]. Economic Geology, 98: 1 371~1 396.

Viets J G, Hofstra A H, Emsbo P, *et al*. 1996. The composition of fluid inclusions in ore and gangue minerals from the Silesian-Cracow Mississippi Valley-type Zn-Pb deposits Poland: Genetic and environmental implications [J]. Prace-Panstwowego Instytutu Geologicznego, 154: 85~103.

Volozh Y, Talbot C and Ismail-Zadeh A. 2003. Salt structures and hydrocarbons in the Pricaspian basin[J]. AAPG Bulletin, 87: 313~334.

Wallace M W, Both R A, Ruano S M, *et al*. 1994. Zebra textures from carbonate-hosted sulfide deposits; sheet cavity networks produced by fracture and solution enlargement[J]. Economic Geology, 89: 1 183~1 191.

Waltham T, Bell F G, Culshaw M G, *et al*. 2005. Sinkholes and subsidence: Karst and cavernous rocks in engineering and construction[J]. Environmental & Engineering Geoscience, 2(11): 180~191.

Wang A J, Peng Q M and Palmer M R. 1998. Salt dome-controlled sulfide precipitation of Paleoproterozoic Fe-Cu sulfide deposits, eastern Liaoning, northeastern China[J]. Economic Geology, 93(1): 1~14.

Warren J K. 1996. Evaporites, brines and base metals: What is an evaporite? Defining the rock matrix[J]. Australian Journal of Earth Sciences, 43(2): 115~132.

Warren J K. 2000. Evaporites, brines and base metals: Low-temperature

ore emplacement controlled by evaporite diagenesis[J]. Australian Journal of Earth Sciences, 47(2): 179~208.

Warren J K. 2016. Evaporites: A Geological Compendium[M]. New York, N.Y., Springer.

Warren J K and Kempton R H. 1997. Evaporite sedimentology and the origin of evaporite-associated Mississippi Valley-type sulfides in the Cadjebut mine area, Lennard shelf, Canning basin, Western Australia[J]. SEPM Special Publication, 57: 183~205.

Wilkinson J J. 2014. Sediment-hosted zinc-lead mineralization: Processes and perspectives[J]. Treatise on Geochemistry: Second Edition, 13: 219~249.

Williams P J, Barton M D, Johnson D A, *et al*. 2005. Iron oxide copper-gold deposits geology, space-time distribution, and possible modes of origin[J]. Economic Geology, 100: 371~406.

Xu Hong and Cao Jifu. 2001. Meta-evaporite and signification in Paleoproterozoic Terrene in eastern Liaoning Province[J]. Global Geology, 20(2): 124~132 (in Chinese with English abstract).

Xue C J, Zeng R, Liu S W, *et al*. 2007. Geologic, fluid inclusion and isotopic characteristics of the Jinding Zn-Pb deposit, western Yunnan, South China: A review[J]. Ore Geology Reviews, 31(1~4): 337~359.

Yardley B W D. 2005. 100th Anniversary Special Paper: Metal concentrations in crustal fluids and their relationship to ore formation[J]. Economic Geology, 100: 613~632.

Yu Yixin, Zhou Xinhuai, Peng Wenxu, *et al*. 2011. An overview on salt structures[J]. Geotectonica et Metallogenia, 35(2): 169~182 (in Chinese with English abstract).

Yuan Bo, Mao Jingwen, Yan Xinghu, *et al*. 2014. Sources of metallogenic materials and metallogenic mechanism of Daliangzi ore field in Sichuan Province: Constraints from geochemistry of S, C, H, O, Sr isotope and trace element in sphalerite[J]. Acta Petrologica Sinica, 30(1): 209~220 (in Chinese with English abstract).

Zhou J X, Gao J G, Chen D, *et al*. 2013. Ore genesis of the Tianbaoshan carbonate-hosted Pb-Zn deposit, Southwest China: Geologic and isotopic (C-H-O-S-Pb) evidence[J]. International Geology Review, 55: 1 300~1 310.

Zhuang L L, Song Y C, Leach D L, *et al*. 2023. Vanished evaporites, halokinetic structure, and Zn-Pb mineralization in the world-class Angouran deposit, northwestern Iran[J]. Geological Society of America Bulletin, 136: 1 569~1 586.

Zou Caineng, Du Jinhu, Xu Chunchun, *et al*. 2014. Formation, distribution, resource potential and discovery of the Sinian-Cambrian giant gas field, Sichuan Basin, SW China[J]. Petroleum Exploration and Development, 41(3): 278~293 (in Chinese with English abstract).

附中文参考文献

戈红星, Jackson M P A. 1996. 盐构造与油气圈闭及其综合利用[J]. 南京大学学报(自然科学版), 32(4): 640~649.

黄世强. 2019. 金顶超大型铅锌矿床有机流体与围岩/蒸发岩的相互作用及其对成矿的意义[D]. 北京: 中国地质大学(北京).

贾承造, 赵文智, 魏国齐, 等. 2003. 盐构造与油气勘探[J]. 石油勘探与开发, 30(2): 17~20.

金之钧, 龙胜祥, 周　雁, 等. 2006. 中国南方膏盐岩分布特征[J]. 石油与天然气地质, 27(5): 571~583.

金之钧, 周　雁, 云金表, 等. 2010. 我国海相地层膏盐岩盖层分布与近期油气勘探方向[J]. 石油与天然气地质, 31(6): 715~724.

刘家军, 柳振江, 杨　艳, 等. 2007. 盐类在金属、非金属成矿过程中的作用[J]. 地质找矿论丛, 22(3): 161~171.

刘静江, 李　伟, 张宝民, 等. 2015. 上扬子地区震旦纪沉积古地理[J]. 古地理学报, 17(6): 735~753.

单秀琴, 张　静, 张宝民, 等. 2016. 四川盆地震旦系灯影组白云岩岩溶储层特征及溶蚀作用证据[J]. 石油学报, 37(1): 17~29.

许　虹, 曹积富. 2001. 辽东古元古宙成矿带中的变质蒸发岩及其意义[J]. 世界地质, 20(2): 124~132.

余一欣, 周心怀, 彭文绪, 等. 2011. 盐构造研究进展述评[J]. 大地构造与成矿学, 35(2): 169~182.

袁　波, 毛景文, 闫兴虎, 等. 2014. 四川大梁子铅锌矿成矿物质来源与成矿机制: 硫、碳、氢、氧、锶同位素及闪锌矿微量元素制约[J]. 岩石学报, 30(1): 209~220.

邹才能, 杜金虎, 徐春春, 等. 2014. 四川盆地震旦系-寒武系特大型气田形成分布、资源潜力及勘探发现[J]. 石油勘探与开发, 41(3): 278~293.